Abstract

Department of Aeronautics

Imperial College London

The behavior of II/III mixed-mode delamination in laminated composites and potential savings in Aerospace regarding verification processes

by Oscar CANO IRANZO

Delamination is recognised as the most critical damage process in laminated composites: even a simple, single plane defect can result in multi-plane delamination growth (delamination migration) which is often associated to other secondary processes such as intralaminar or translaminar damage. In previous research, the link between the mode III component and delamination migration was established [9]. However, the exact mode-mixity at which this migration occurs needs to be investigated further.

This project will determine the effect of load introduction on the migration threshold in II/III mixed-mode delamination. The test method that will be used is a 6-point bending plate [10] that relies on bending moments to induce mixed-mode delamination. The tests will be instrumented with acoustic emission to capture, if possible, the onset of resin microcracking. The test will then be interrupted for detailed fractographic analysis at the crack front. These will give an insight of the role of bending on the fracture process of mode II-III on multi-angled interfaces.

Acknowledgements

I would like to express my sincerest gratitude to Prof. Greenhalgh, Prof. Robinson and Dra. Canturri not only for their supervision and valuable advice during the whole duration of this project but also for giving me the opportunity to introduce myself into the challenging world of composites field.

To Mr. Gary Senior, Mr. Jonathan Cole and Mr. Keith D Wolstenholme for their support with manufacturing and testing the composite test specimens and for their kindness.

I would also like to thank Jose B. Parra for giving me the opportunity to undertake my Master's thesis at Imperial College London and also both my colleagues from UPC and ICL (Ned, Carlos, Jorge, Martín, David and Joan) not only for the long working hours but also for the shared good moments.

Finally, I cannot express how incredibly grateful I feel for my parents' and Barbara's unconditional support in the down moments throughout these six years. Without you, none of this would have ever been possible.

Contents

List of Figures

Nomenclature

Symbol	Description	*Units*
ε	Strain	-
G	Shear Modulus of elasticity	MPa
E	Young's Modulus	J/m^2
G_I	Mode I strain energy release rate	J/m^2
G_{II}	Mode II strain energy release rate	J/m^2
G_{III}	Mode III strain energy release rate	J/m^2
G_{IC}	Critical mode I strain energy release rate	J/m^2
G_{IIC}	Critical mode II strain energy release rate	J/m^2
G_{IIIC}	Critical mode III strain energy release rate	J/m^2
h	Specimen half thickness	mm
L	Element lenght	mm
ν	Poisson's Ratio	$-$
ρ	Material density	g/m^3
U_I	Nodal displacement in mode I	mm
U_{II}	Nodal displacement in mode II	mm
U_{III}	Nodal displacement in mode III	mm

Abreviations

6PBP	Six Point Bending Plate
FE	Finite Elements
SERR	Strain Energy Release Rate
VCCT	Virtual Crack-Closure Technique

Chapter 1

Introduction

1.1 Motivation

The route to certification of composite aircraft structures is identified as a very costly procedure due to the huge amount of testing involved in the different steps of the verification procedure. To be competitive in the future and maintain and hopefully increase the European share of the commercial aircraft market it is necessary to reduce this cost. This requires a new less test demanding verification procedure.

The two main goals are, on one hand, reach an analysis based procedure for structural verification from design to final certification by concentrating on the development of design and analysis methods in order to reduce the tremendous amount of testing and to optimise testing still required and thereby save costs and shorten the time spent in testing. On the other hand, roughly size the potential saving that could be obtained

In this thesis, it has been used the FE Software ABAQUS 6.14-1 to simulate the behavior of a IM7/8552 carbon fibre specimen in a 6PBP test as a analytical technique in preference to futures tests.

1.2 Edavcos

The EDAVCOS programme was the first stage towards a common cost efficient verification procedure. The targets savings for the new verification procedure were 50% reduction of the total cost for verification and 60% reduction of the time scale. By providing improved design and analysis methods, approaches for more efficient testing and recommendations for future research and development could be achieved, EDAVCOS significantly contribute to future development of efficient (low cost low weight) composite aircraft structures.

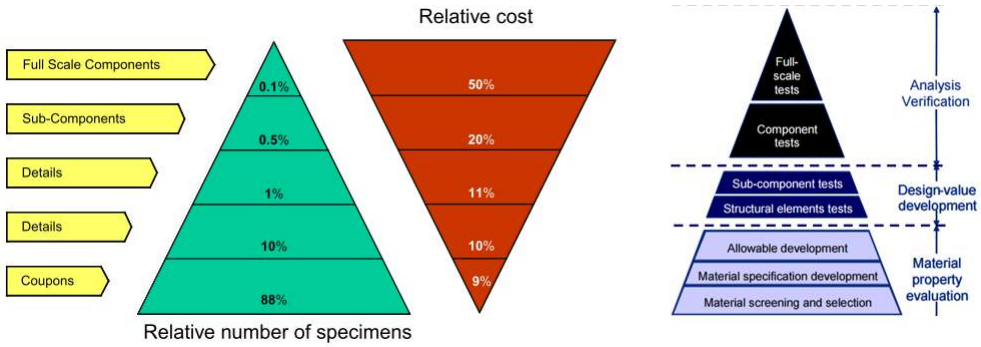

Figure 1.1: Qualification testing and cost pyramids[1][3]

1.3 Delamination of composite materials

High performance composites usually found in a laminated structure i.e. they are manufactured by stacking several layers or plies one on top of the other. Delamination is a mode of failure for composite materials that consists in ply debonding forming a mica-like structure of separate layers. Delaminations can be caused for example by cyclic stresses and repeated impacts of foreign bodies, in the case of the engines blades, that body impact would be the impact of a bird.

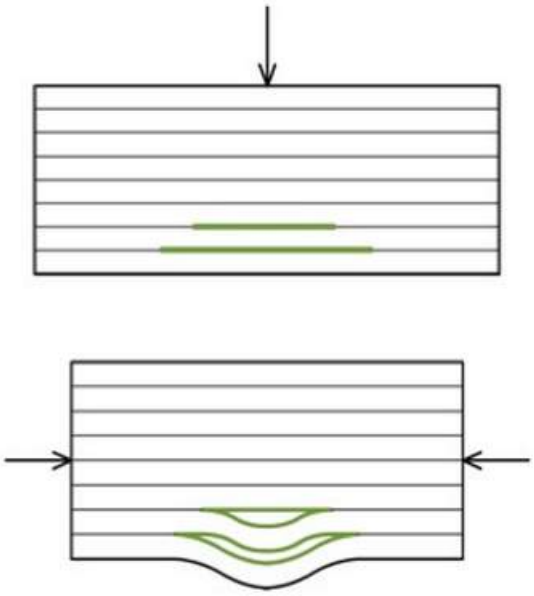

Figure 1.2: Graphic representation of delamination in composite materials

This failure mode is considered as a particular gradual failure mode due to it may

cause dramatic losses of structural performance by promoting delamination buckling under compression loads. The resistance of the delamination is characterised by the strain-energy release rate G.

1.3.1 Strain energy release rate

The strain energy release rate (or simply energy release rate) is the energy vanished throughout the fracture per unit of newly created fracture surface area. The energy that must be supplied to a crack tip for it to grow must be balanced by the amount of energy dissipated due to the formation of new surfaces and other dissipative processes such as plasticity.

There are three ways of applying a force to enable a crack to propagate:

- **Mode I** – Opening mode, a tensile stress normal to the plane of the crack.
- **Mode II** – Sliding mode, a shear stress acting parallel to the plane of the crack and perpendicular to the crack front.
- **Mode III** – Tearing mode, a shear stress acting parallel to the plane of the crack and parallel to the crack front.

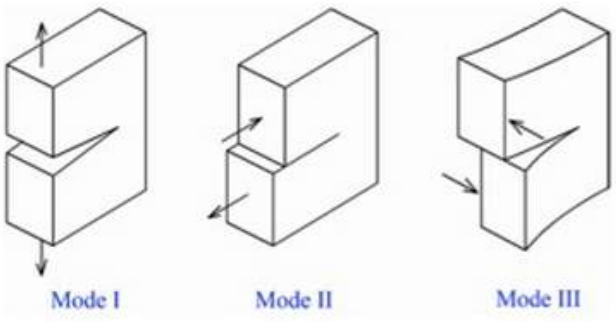

Figure 1.3: Strain energy release rate modes

1.4 Softwares used

1.4.1 Creo Parametric 2.0

Creo Parametric 2.0 is a 3D CAD software that delivers powerful design functionality with a intuitive user interface to speed the design process and make you instantly productive. It is going to be used in this project to design the six-point bending point test's fixtures based on the fixtures used by [10] and adding two degrees of freedom, one on each axis (X,Y). The engineering drawing could be find at (Appendix A).

1.4.2 Abaqus 6.14-1

ABAQUS is a software suite for finite element analysis and computer-aided engineering. It is commonly used in different industries such as automotive and aerospace. The product is popular with academic and research institutions due to the wide material modeling capability, and the program's ability to be customized.

This tool has been used to model the six-point bending plate specimens. Once got familiar with the FE Software, through the virtual crack closure technique also known as VCCT, the strain energy release rate (G) was obtained. A tailor-made Abaqus tutorial could be find at (Appendix B). One of the problems to be emphasised, is the restricted access due to working with the student version, which limited the simulations to less than 250.000 nodes. To avoid this problem, a symmetry was done, so the half of the nodes were not necessary any more.

1.4.3 Laminate Analysis Program (LAP)

Laminate Analysis Program is software tool for the analysis and design of composite material laminates. This tool has been used in preliminary design for tailoring the stacking sequences, then analyzing the composite component with other methods such as finite elements (Abaqus), and finally optimising the design by inspecting the laminate behavior layer by layer.

It is well-known and widely-used tool, due to its fast user-friendly usability. Further details, tutorials and downloads can be found in the official web page

Chapter 2

Literature review

2.1 Delamination

2.1.1 Introduction

To review the state of the art in knowledge of delamination behavior a literature review was undertaken. The survey focused on the previous mode fracture studies/configurations that had already been done to study the delamination.

- **Mode I and mode II**: Many studies have been conducted on mode I and mode II using the Double Cantilever Beam (DCB) and End-Notched Flexure (ENF) tests. Those tests are universally accepted [14][14].

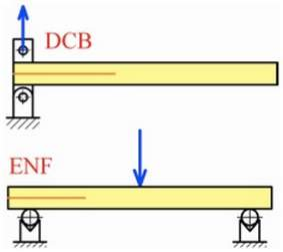

Figure 2.1: Double Cantilever Beam (DCB) and End-Notched Flexure (ENF) tests[11].

- **Mode III:** Most researchers consider the Edge Crack Torsion (ECT) test the most adequate for measuring GIIIc. However, the validity of many results has been questioned due to non-linearity and specimen geometry dependence. Further investigation is required. [14, 15, 16, 17]

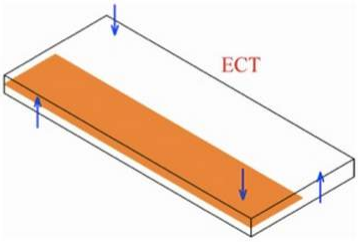

Figure 2.2: Edge crack torsion (ECT) test[12].

- **Mixed-mode I + II:** The mixed-mode bending (MMB) test standardised by ASTM is considered the best method for characterising delamination in mixed-mode I + II. In fact, the MMB test can be viewed as the combination of the DCB and ENF tests. Nevertheless, work reported often revealed inconsistencies in experimental results. [18, 19]

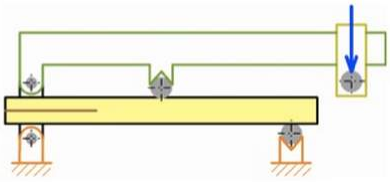

Figure 2.3: Mixed-mode bending (MMB) test[11].

- **Mixed-mode I + III:** Very little work has been reported on delamination under mixed mode I + III. A new test method called 8-point bending plate had been developed.

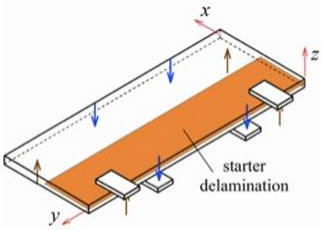

Figure 2.4: Eight-point bending plate (6PBP) test [13].

- **Mixed-mode II + III:** Very little work has been reported on delamination under mixed mode II + III. From the research conducted by [10], six-point bending plate (6PBP) specimens with cross-ply lay-up and a standard 0/0 interface were selected. It

has also been investigated by Szkrenyes[20]. Szekreynes used a unidirectional (UD) pre-stressed end-notched flexure (PENF) specimen that combines an initial split cantilever beam type mode III loading with a subsequent mode II bending one.

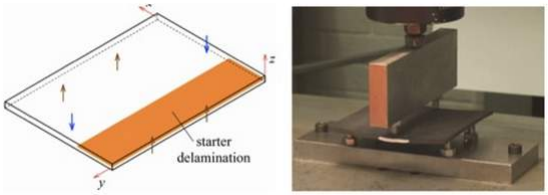

Figure 2.5: Six-point bending plate (6PBP) test [10].

2.1.2 Delamination starting

A shear stress is the responsible of transferring the stress to the resin, initiating a damage at the inter laminar region. To put it in another words, the fibers in a composite material that are expose to mode II loading form ahead of the crack a series of micro-cracks. In terms of fractography, these micro-cracks can be identified and differentiate pure mode I delamination to mixed-mode delamination.

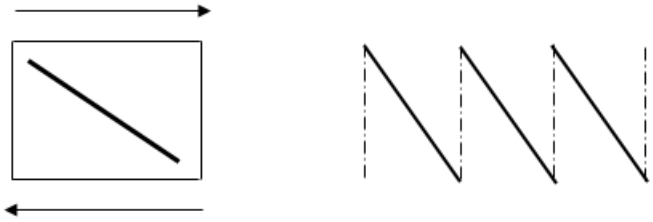

Figure 2.6: Two-dimensional model of shear deformation at the crack.

Chapter 3

Layup

3.1 Layup methodology and materials

This section describes the methods used for the manufacture of the test panels. The material used was Hexcel IM7/8552 (0.125 mm ply thickness) pre-preg. The properties of this material are described in Appendix C. The six-point bending plate panels used were hand laid-up. During lay-up, every set of 5 plies was compacted in a vacuum table. A 10 µm PTFE film was inserted between the two halfs of the panel as a starter delamination. The film was cut with a scalpel.

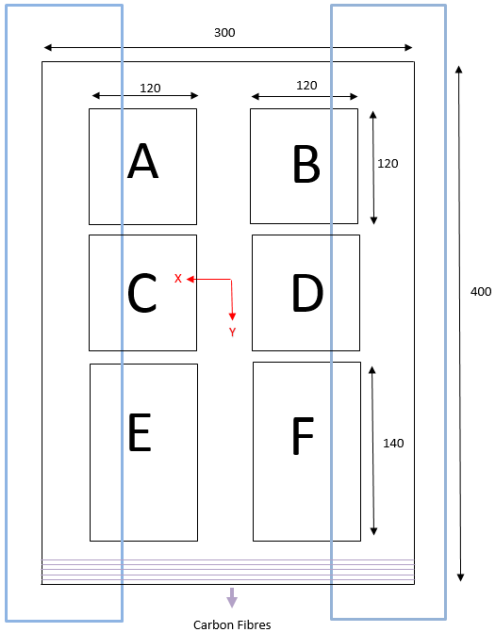

Figure 3.1: Specimens lay-out within the lay-up

The Specimens lay-out within the layup is represented in [Figure 3.1]. In order to avoid problems in the edges, the panels were oversized by 15 mm around the panel and the size of cutting blade was also accounted for. Panels were cured in an LBBC Quicklock Autoclave. Finally, the specimens A,B,C,D,E,F represented below [Figure 3.1] were cut with a circular saw.

The stacking sequences examined in this thesis are two. Both of them were analysed with the software LAP (Laminate analysis composites). On one hand, Configuration Morais: 90/90; 30 plies; 0,15mm/ply; 2h=3.9mm Dc=0.0010285; Global & partial symmetric:

[(90/0)][(90/0)(90/0)(90/0)] [(0/90)(0/90)(0/90)] [(0/0)] [(90/0)(90/0)(90/0)] [(0/90)(0/90)(0/90)][(0/90)].

On the other hand, the Configuration 2: 90/90 II 0/0; 32 plies; 0,125mm/ply; 2h=4mm Dc= 0.0010458; Global asymmetric & partial symmetric. This is the configuration selected for testing.

[(90/0)(90/0)(90/0)(90/0)] [(0/90)(0/90)(0/90)(0/90)] [(0/90)(0/90)(0/90)(0/90)] [(90/0)(90/0)(90/0)(90/0)].

Chapter 4

Results

4.1 Theoretical analysis and results

The main goal of the development of the present test was to generate both mixed modes II + III by bending. 6PBP specimens were contemplated as a practical solution since the test involves simultaneous bending along the length and width directions. The configuration below stimulates delamination growth near the ends. Additionally, the configuration shown was able to provoke high mode III when small D and high L values are chosen. It is worth highlighting the 0°corresponds to the x axis and the 90°corresponds to the y axis.

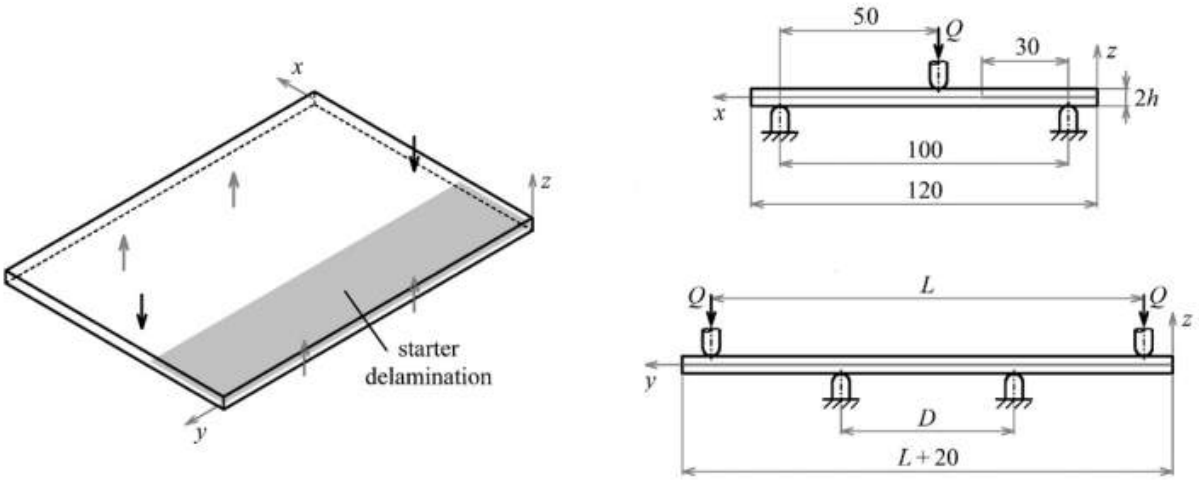

Figure 4.1: Geometry of 6PBP specimen. Perspective (left), front (Bottom) and side (top) views [13].

An FE model was created in the ABAQUS to simulate only the half of the specimen as it was symmetric (Appendix B). The results were extracted using the Virtual Crack Closure Technique (VCCT) which showed that $G_I \approx 0$ and also that the analysis deals with mode II and mode III components.

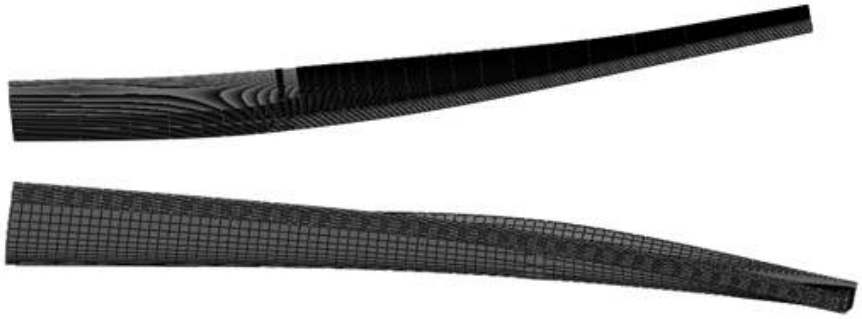

Figure 4.2: FE model: Views of the deformed configuration in the yz (top) and xz (bottom) planes

Different configurations can be specified to cover a broad scope of mode II + III mixity by varying L and D values. This study focused on the three combinations showed below. These three configurations were designated as 6PBP(18), 6PBP(30) and 6PBP(42) due to the $G_{III}/G(\%)$ ratio. Specimens 1 and 3 (15%); Specimens 2 and 4 (30%); Specimens 5 and 6 (42%).

L	D	G_{III}/G (%)	# Specimens
100	60	18	2
100	40	30	2
120	65	42	2

Figure 4.3: Specimen configurations and number of specimens tested.

The strain energy release rate distributions of G_I, G_{II} and G_{III} obtained with the FEA showed considerable non-linearity which is manifested in the plots below. It should be mentioned that 0.9*G was considered to extract the $G_{III}/G(\%)$ values to avoid the non-linearity. The failure criteria formula is based on [22].

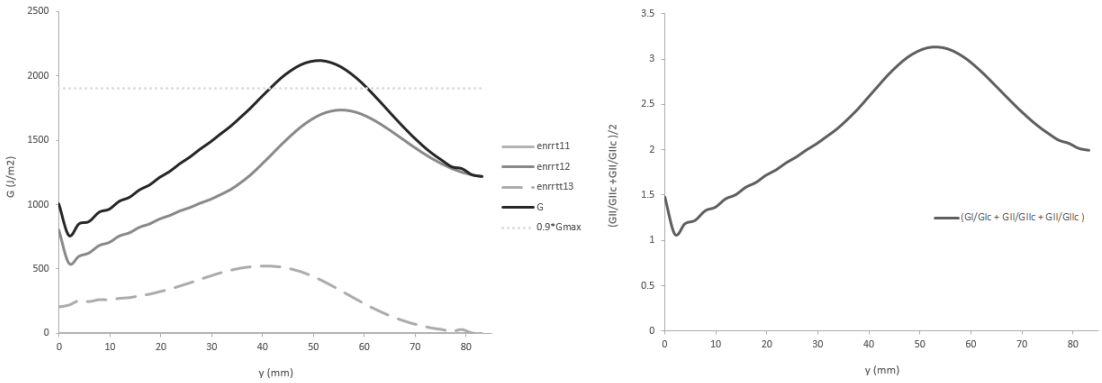

Figure 4.4: Distributions of $G_{I,}$, $G_{II,}$ and G_{III} along the delamination on 6PBP(18) (left) and failure criteria $(G_I/G_{Ic} + G_{II}/G_{IIc} + G_{III}/G_{IIIc})$ (right).

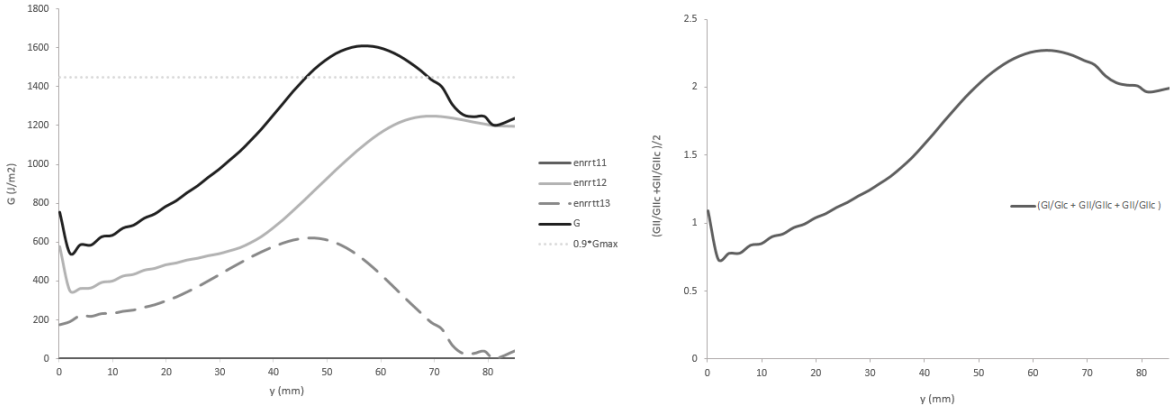

Figure 4.5: Distributions of $G_{I,}$, $G_{II,}$ and G_{III} along the delamination on 6PBP(30) (left) and failure criteria $(G_I/G_{Ic} + G_{II}/G_{IIc} + G_{III}/G_{IIIc})$ (right).

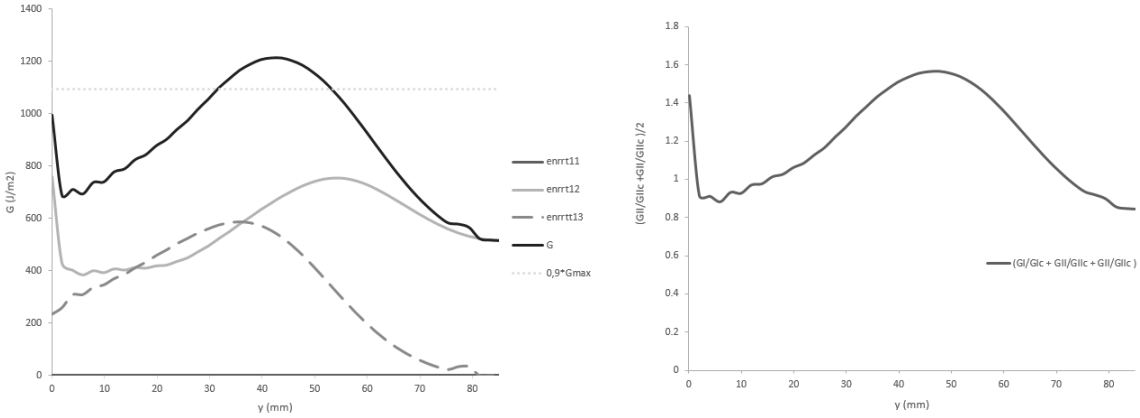

Figure 4.6: Distributions of $G_{I,}$, $G_{II,}$ and G_{III} along the delamination on 6PBP(42) (left) and failure criteria ($G_I/G_{Ic} + G_{II}/G_{IIc} + G_{III}/G_{IIIc}$) (right).

4.2 Experimental analysis and results

The six point bending plate's specimens were obtained from laminated plates by hot pressing according to processing conditions and characteristics mentioned in the Chapter 3. High-strength screws acted as supports and load points with spherical heads were used in the test rig (Appendix A). Tests were carried out in a Instron 50kN machine at 2mm/min. The fixtures design was inspired by the 6PBP fixtures used in [10]. Moreover, two degrees of freedom were aded on the fixtures, one on each (y specimen's direction).

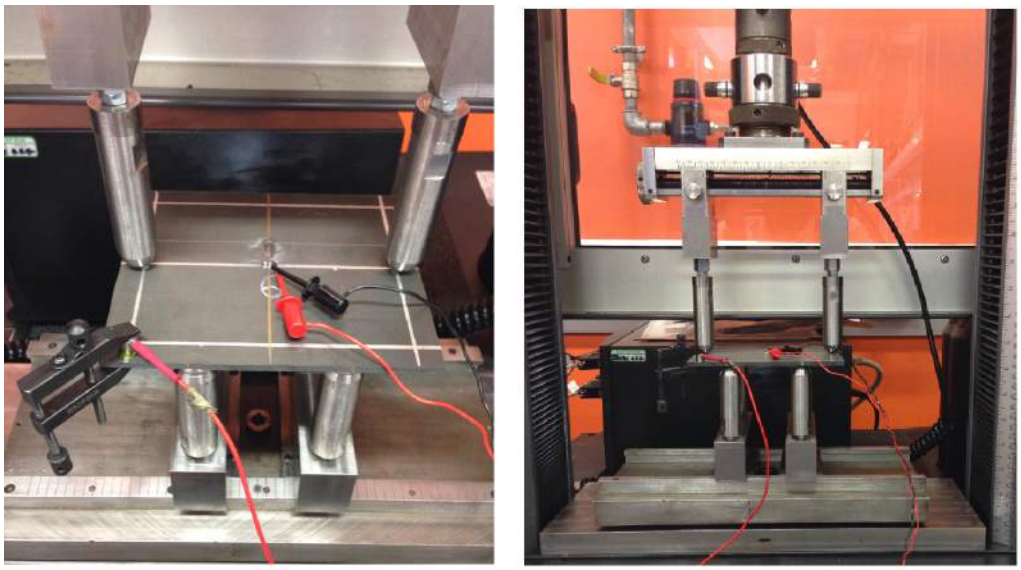

Figure 4.7: Pictures of the test setup.

The figures below shows typical load-displacement curves and the G_{III}/G distribution along the delamination from 6PBP(18), 6PBP(30) and 6PBP(42).

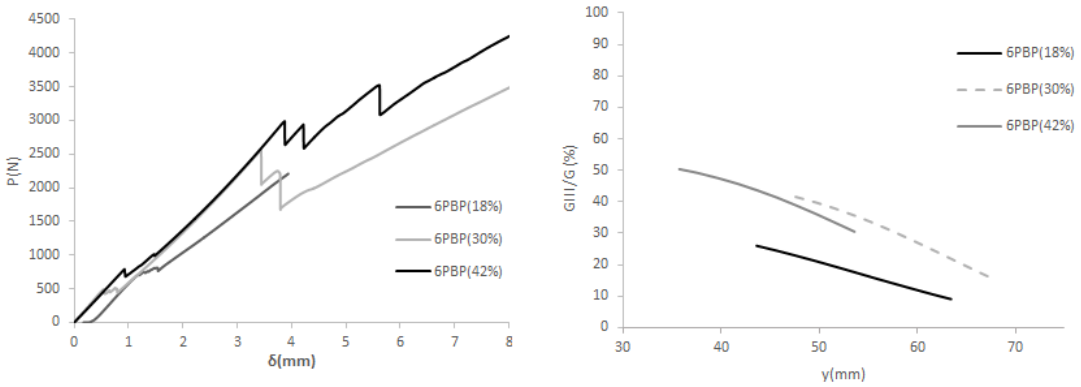

Figure 4.8: Load-displacement curves (left) and distribution along the delamination (right) from 6PBP(18), 6PBP(30) and 6PBP(42).

4.2.1 Failure Analysis and Instrumentation

4.2.1.1 Acoustic Emission results

This Non-Destructive Testing (NDT) method was used to analyse emitted sound waves caused by the discontinuities. These acoustic waves were induced by small deformations and cracking, which occurred prior to structure failured.

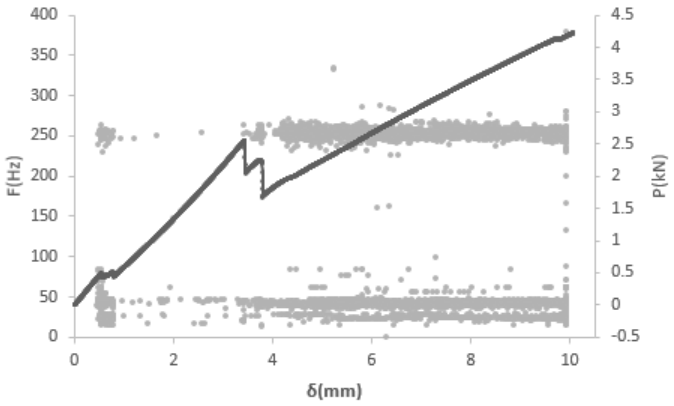

Figure 4.9: Representative Acoustic Emission result: Specimen 4, first test (left) and second test (right).

4.2.1.2 Ultrasonic inspection result

The TOF C-Scans revealed the presence of multi-plane delamination in specimens S1-S6. However, ply splits were generally not well captured with C-Scans and these were later analysed X-radio-graphically. The Triton 1800 immersion tank provided by Technitest was utilised to undertake the C-Scan. The C-Scan was used different times (after the panel was cured, once the specimens were cut with the circular saw and once all the specimens were tested). A coin was used as a reference in each C-Scan. The results from the C-Scan analysis are presented in Appendix E.

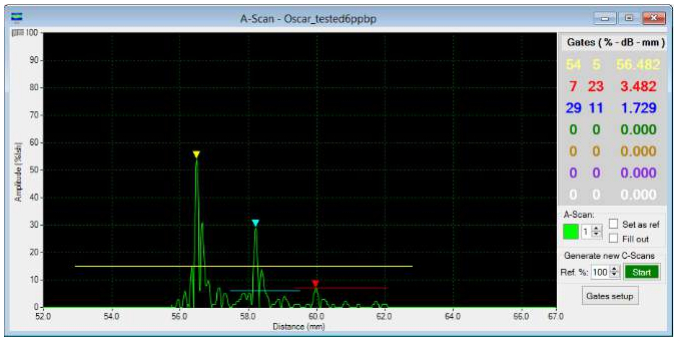

Figure 4.10: C-Scan: Front-face signal (yellow), teflon signal (blue) and back-face signal (red).

It is worth highlighting the usage of Dolphi Cam as a portable ultrasonic inspection tool (Appendix D). This instrument was used to check how the delamination propagated in each test, as it is a portable tool, it could be used whenever was desired. It allowed us to know if we should keep on testing or not as delamination state could be known instantly. However, this observation should be taken carefully to analyse the delamination growth.

4.2.1.3 X-Radio-graph inspection results

The specimens S1-S2-S3 were selected. The results from the analysis can be shown in Figures 4.15 and 4.16. As can be seen in Figures below and after comparing with the corresponding C-Scan, ply splitting was not observable.

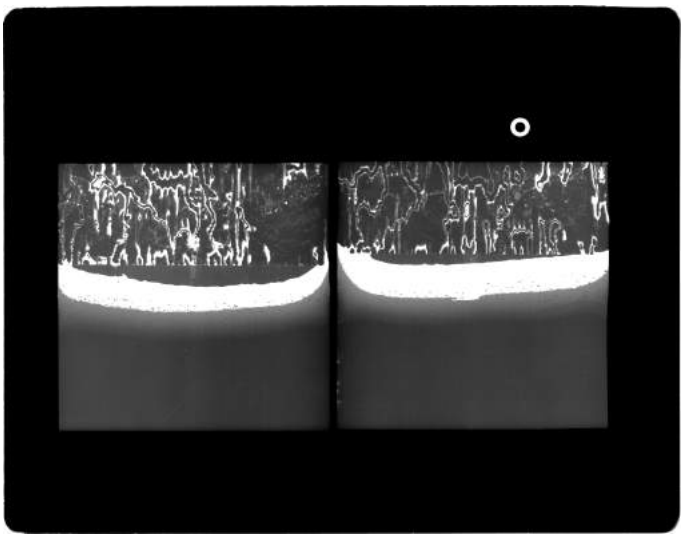

Figure 4.11: X-Ray: Specimen 1 (lets) and specimen 2 (right).

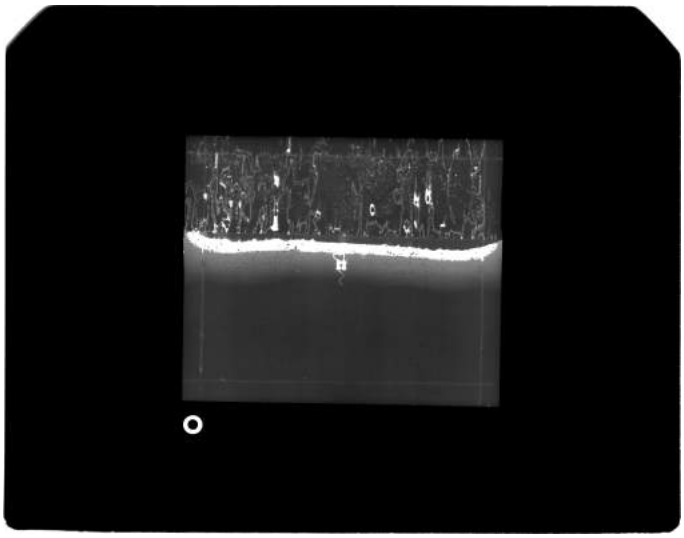

Figure 4.12: X-Ray: Specimen 1 (left) and specimen 2 (right).

4.2.1.4 Optical microscopy results

Nine specimens were cut and selected for the photo microscopic evaluation on the ZEISS AX10 Imager.M2m microscope: three from each specimen (S1-S2-S5). Figure F.1 illustrates the location of each section within the original specimen. A MURG 24-BB saw was used to cut each specimen. Each section was potted in Polyester casting resin, then ground and polished using standard techniques. Reflected light differential contrast microscopy was used

to examine the cross sections, and photomicrographs were taken at different magnifications across the entire width of each specimen. The specimens were always placed in order that the top face, where the load had been applied, was on top of each picture done.

Moreover, considering the photomicrographs that follow in the Appendix F, there was no preference observed for the initiation of the matrix cracks from the intralaminar voids.

When comparing Figs. 2-10, it is evident that these cracks vary in length and spacing from specimen to specimen. This was also true from location to location within a specimen (three possible locations).

To determine whether there was any correlation between observed matrix cracking and location of the section, the nine sections from the three different specimens were evaluated. No correlations were found between the shape/length of the matrix crack and the section location.

The above observations indicate that matrix cracks are present at the delamination in all three configurations chosen to do the six point bending plate test (6PBP(18), 6PBP(30), 6PBP(42)).

4.2.1.5 Scan Electron Microscope (SEM)

Visual inspection on the opened surfaces were undertaken with the HITACHI S-3700N Scan Electron Microscope reveled the presence of delamination verifying the C-Scan results. Each section was cut and then opened manually, showed in Fig. G.11. The specimens analysed were always placed in the same position to take into account the fibre direction and the starter delamination location. Results can be found in Figs. G.12-G.17. The results obtained from these analysis do not clearly permit to distinguish between the fibre dominated section and the matrix dominated section. In the Figs. G.12-G.17 can be easily find cusps regardless the dominance.

Chapter 5

Analysis of potential verification costs savings

This section proposes a new approach to potential cost savings estimation related to the verification of composite structures in the Aerospace Industry. It should be noted that the subscript 'i' denote the aircraft model, regarding the formula there are 'N' different types of aircraft included in the analysis such as Airbus S.A A320,A380 or The Boeing Company 787.

The sub index 'j' indicates either if it is a ***primary structure*** (j=1) or a ***secondary structure*** (j=2). The airworthiness standards define on one hand *primary structures* as those that would endanger the aircraft upon failure such as the wings, load-bearing portions of the fuselage, the empennage and control surfaces. On the other hand, *secondary structures* as those that do not cause immediate danger upon failure, for example the fairings, cowlings, baffles, unpressurized cabin doors or access panels.

The knowledge both obtained on different management lectures [6, 7, 8] received at Etseib, Universitat Politecnica de Catalunya (UPC) and on the strategical case study book[5] has been applied not only in order to figure out a framework, which have been though as a market size problem, but also to create a mathematical model to get approximations both on the global cost that verification procedures generate and potential saving that can be obtained trough the simulation instead of full procedure testing.

5.1 Mathematical Model

5.1.1 Target Functions

1. The function that determines the approximate **Global Verification cost** in the Aeronautics field in k(£) is:

$$VerificationCost = \sum_{j}^{2}\sum_{i}^{N}(FC_{ij} + VC_{ij}) = \sum_{j}^{2}\sum_{i}^{N}[FC_{ij} + (\frac{CP_{ij}}{100} * MA_i * C_{ij} * \alpha_{ij})]$$

$[\forall i = 1...N;\ \forall j = 1...2]$

2. The function that determines the approximate **Global Potential Saving Cost** in k(£) is:

$$PSC = \sum_{j}^{2}\sum_{i}^{N}\beta_{ij} * FC_{ij} + \sum_{j}^{2}\sum_{i}^{N}\gamma_{ij} * (\frac{CP_{ij}}{100} * MA_i * C_{ij} * \alpha_{ij})\ \ [\forall i = 1...N;\ \forall j = 1...2]$$

5.1.2 Datum

- CP_i : Composite Structural Weight in each aircraft model 'i' [%] [4].

5.1.3 Variables

- $\mathbf{C}_{ij}$: Verification cost regarding the structure type 'j' of an 'i' aircraft model in a series production [k(£)] $[\forall i = 1...N;\ \forall j = 1...2]$.
- $\mathbf{CP}_i$: Composite Structural Weight regarding the structure type 'j' in each aircraft model 'i' [%]. $[\forall i = 1...N]$.
- $\mathbf{MA}_i$: Predicted quantity of manufactured model 'i' aircrafts [units] $[\forall i = 1...N]$.
- $\mathbf{CV}_{ij}$: Verification cost regarding the structure type 'j' of an 'i' aircraft model [k(£)]. $[\forall i = 1...N;\ \forall j = 1...2]$.
- α_{ij}: Parts per unit of structure type 'j' in the aicraft model 'i'.[%] $[\forall i = 1...N;\ \forall j = 1...2]$.
- $\mathbf{FC}_i$: Costs that implies launching a new aircraft 'i'[k(£)] $[\forall i = 1...N]$.
- $\mathbf{FC}_{ij}$: Fixed verification costs generated associated to the structure 'j' on the aircraft 'i'[k(£)]

$[\forall i = 1...N;\ \forall j = 1...2]$.

- $\mathbf{VC}_{ij}$: Variable costs regarding a series production [k(£)]. $[\forall i = 1...N;\ \forall j = 1...2]$.
- **PSVC**: Potential Saving Verification Cost that can be obtained trough the simulation instead of full procedure testing[k(£)].
- β_{ij}: Verification saving cost that would be obtained from the structure type 'j' when launching an aircraft model 'i' [%] $[\forall i = 1...N;\ \forall j = 1...2]$.
- γij: Verification saving cost that would be obtained from the structure type 'j' when manufacturing per aircraft model 'i' [%] $[\forall i = 1...N;\ \forall j = 1...2]$.

5.1.4 Restrictions

- $\sum_j^2 \alpha_{ij} = 1 \quad [\forall i = 1...N]$; For each aircraft model 'i'the sum of both structures must be 1.
- $\sum_j^2 \mathrm{CP}_{ij} \leq C_i \quad [\forall i = 1...N]$; The sum of both structural composite must be at maximum CP_i
- $\mathrm{CP}_i \leq 100 \quad [\forall i = 1...N]$; For each aircraft model 'i' the maximum percentatge of composite is the total amount of the aircraft.
- $\beta_{ij} >> \gamma ij\ [\forall i = 1...N]$; The launching cost is much more costly than the unitari cost in a series production.

5.1.5 Analysis Assumptions:

1. The analysis has been focused on both Civil and Military Aircfrafts.
2. The market could be represented by '18' diferent types of aircraft; i=18.
3. There exists a direct relation between the composite structural weight and the verification cost associated. The analysis will be focused on the commercial transport and military applications up to the year 2010.

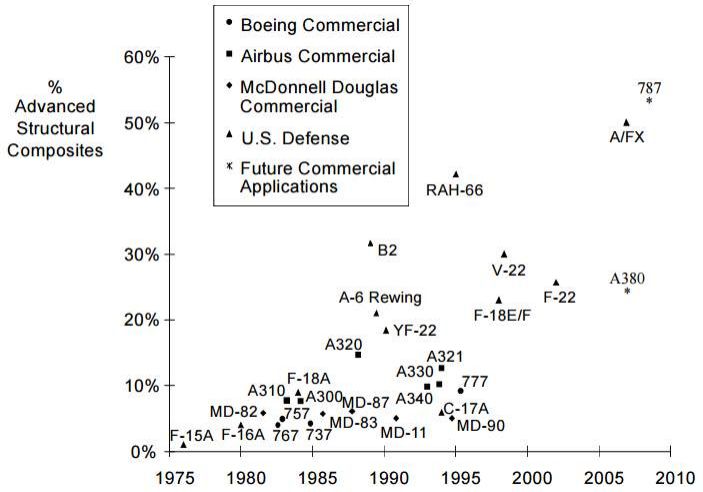

Figure 5.1: Presented by L. Ilcewicz at 11/10/09 Montana State Univ. Seminar[4]

4. FC_i= Average Cost that means launching an Aircraft = 200M$ = £140.000k.

5. The total quantity of planes that are expected to be manufactured of each Aerospace model 'i' is: $MAi = \frac{\sum MAi}{\sum i}$.

6. The total quantity of planes that are expected to be manufactured is based on the trend reflected in *[2, 3]*. (Approximately +2% Growth/year).

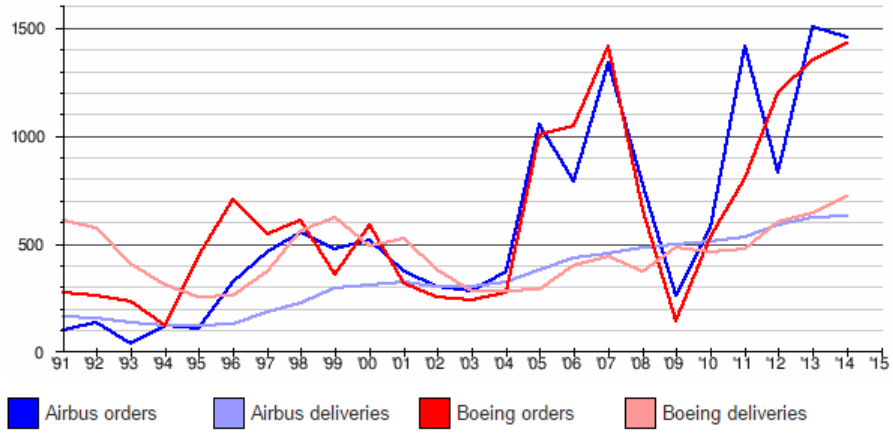

Figure 5.2: Annual net orders recorded and delivered aircraft by Airbus and Boeing[2][3]

5.2 Numerical Hypothesis

Three different hypothesis with different local assumptions will be considered in order to get into a numeric result in three different scenarios.

5.2.1 Hypothesis 1

$-\alpha_{i1} = \alpha_{i2}$=0.5; $\beta_{ij} = 0.3$; γij=0.4

$-FC_{i1}$ & FC_{i2} represent a 20% and a 10% of the launching cost aircraft model 'i'.

$-C_{i1} = \frac{1}{1000} * FC_{i1}$ and $C_{i2} = \frac{1}{1000} * FC_{i2}$; The variable verification cost regarding each aircraft manufactured in series production is approximately a thousand times less than the fixed cost of verification when launching an aircraft.

−Only 25% of the aircrafts that are in the list are launched annually.

Table 5.1: Hypothesis of potential verification costs savings 1

i	Aerospace Model	FC_{i1}[k£]	FC_{i2}[k£]	CPi (%)	MAi [units]	C_{i1}[k£]	C_{i2}[k£]
1	787	28,000	14,000	55	10	28	14
2	A/FX	28,000	14,000	50	10	28	14
3	RAH-66	28,000	14,000	45	10	28	14
4	V-22	28,000	14,000	32	10	28	14
5	F-22	28,000	14,000	28	10	28	14
6	A380	28,000	14,000	25	10	28	14
7	B2	28,000	14,000	32	10	28	14
8	F-18E/F	28,000	14,000	25	10	28	14
9	A-6 REWING	28,000	14,000	25	10	28	14
10	YF-22	28,000	14,000	18	10	28	14
11	A340	28,000	14,000	15	10	28	14
12	777	28,000	14,000	10	10	28	14
13	A320	28,000	14,000	18	10	28	14
14	A330	28,000	14,000	10	10	28	14
15	C-17A	28,000	14,000	7	10	28	14
16	MD-90	28,000	14,000	7	10	28	14
17	F-18A	28,000	14,000	11	10	28	14
18	A310	28,000	14,000	9	10	28	14

VerificationCost= $\sum_j^2 \sum_i^N (0.25 * FC_{ij} + VC_{ij}) = \sum_j^2 \sum_i^N [FC_{ij} + \frac{1}{100} * (CP_i * \alpha_{ij} * MA_i * C_{ij})]$ =£210,886.2 k= £1,096.2M/year

Calculus Brief:

*-Fixed cost (i=1): (0.1*140,000+0.2*140,000)*0.25=£ 10,500k ; (total=£ 210,000k).*

*-Variable cost (i=1, j=1): $\frac{55}{100}$ *0.5*10*($\frac{1}{1000}$ *0.1*140,000)=£ 38.5k; (Total=£ 295,4k).*

*-Variable cost (i=1, j=2): $\frac{55}{100}$ *0.5*10*($\frac{1}{1000}$ *0.2*140,000)= £ 77k; (Total=£ 590,8k).*

PSVC= $\sum_j^2 \sum_i^N \beta_{ij} * FC_{ij} + \sum_j^2 \sum_i^N \gamma_{ij} * (\frac{CP_{ij}}{100} * MA_i * C_{ij} * \alpha_{ij}) =$

£210,000*0.3+(295,4+590,8)*0.4=63,000+354,480= £417,480M/year

Chapter 6

Discussion and Future work

According to the results obtained in this thesis, a clear relation between the global loading and the local morphology can not be defined. In addtion, the data gathered from the optical results and the numerical results obtained by FEA is useful to indicate that the amount of ply splits increase as the mode III increase. Although ply splitting was not perceived in the X-Ray results, it could be observed with the Acoustic Emission software and then validated with the optical microscope. The ply splis might be limitated to the sections analysed with the Optical microscope.

It is worth noting that the findings obtained from the acoustic emission study (Appendix A) help to indentify the failure activity started at the 80% of the failure load. In comparison to [9], the findings show that there is a weak difference between the fibre dominated face and the matrix dominated face. The results obtained from the SEM have been unable to provide evidence that exists a variation between the analysed sections A, B and C. The configurations tested do not indicate enough G_{III}/G ratio to get the migration started, it is worth highlighting that in [9]the delamination interface was -45/45 instead of the standard 0/0 delamination interface. This angle variation in the middle interface must be taken into account in terms of discovering the necessary G_{III}/G ratio to get the migration initiated. On the contrary, the findings from this study do support the study conducted by Masaya Miura, Yasuhide Shindo , Tomo Takeda, Fumio Narita [21]. It is possible to hypothesize that the migration initiates increasing the G_{III}/G ratios tested in this study.

At the date of finalisation of the project, several studies have been left opened. Additionally, the results obtained suggest that the research should be followed in a certain direction.

The following future work is suggested:

6.1 G_{III}/G ratio

After getting manufactured the 6PBP fixtures and having tested three different configurations which suggest to increase the G_{III}/G to get the migration initiated, it would be really interesting to repeat the same test and analysis exposed in this thesis with configurations whose G_{III}/G ratio were higher that 42%.

6.2 Stacking sequence

Additionally, another stacking sequences could be performed such as for example a 0/90 delamination interface. These new stacking configurations could be helpul in terms of getting a wide vision when analysing the results and extracting general conclusions.

6.3 FEA Abaqus Model

A mesh convergence could not be done due to the restrictions offered by the Abaqus' student version, which limited the mesh up to two hundred fifty thousand nodes. It would be interesting to work with a non-limited Abaqus version to refine the mesh used to obtain the results exposed in the Figs. 4.4-4.6 and get a mesh convergence study.

6.4 Specimens S3,S4,S6

The findings of the study suggest that would be interesting to open and then analysed the specimens S3,S4 and S6 as they have not been analysed fractographicly yet.

Chapter 7

Conclusions

Six-point bending plate tests were introduced and used to investigate issues related to the mode-mixity mode II + mode III in relation with both migration and delamination on laminated carbon/epoxy composites with cross-ply lay-up and the standard 0/0 delamination interface. Furthermore, a wide range of configurations was obtained by varying the specimens length and the load/ support point positions. However, due to the non-uniform distributions of G_{II} and G_{III}, a characteristic length ($0.9{*}G_{max}$ was defined to establish a G_{III}/G ratio per each configuration. Therefore, each 6PBP configuration requiered a different FEA model.

From the data obtained from the results provided on this thesis, we can see that the mode mixity ratio G_{III}/G should be incremented in terms of migration starting. The configurations tested do not show enough G_{III}/G ratio to get the migration started. However, the results presented in Appendix G indicates that the migration initiation could be about to succes. Based on the cusps orientation, a clear conslusion can not be defined as the cusps can not be clearly recognised as tilt cusps.

Appendix A

Acoustic Emission results

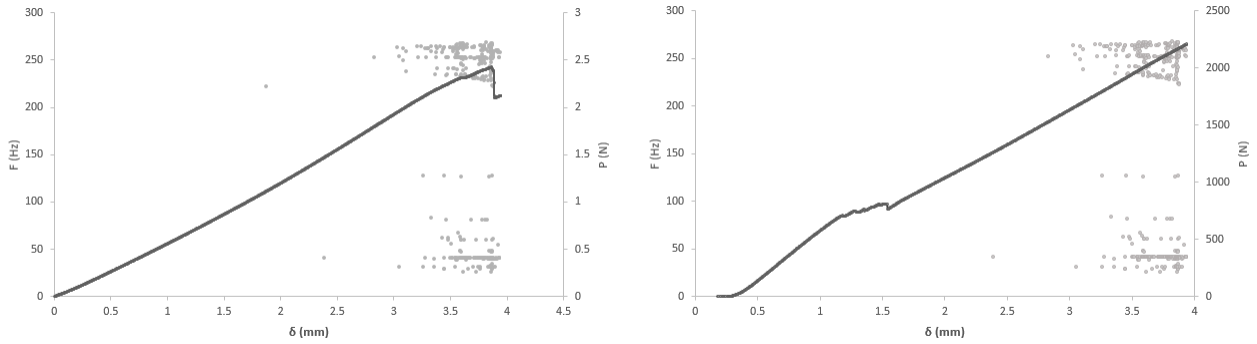

Figure A.1: Acoustic Emission: Specimen 1, fist test (left) and second test (right).

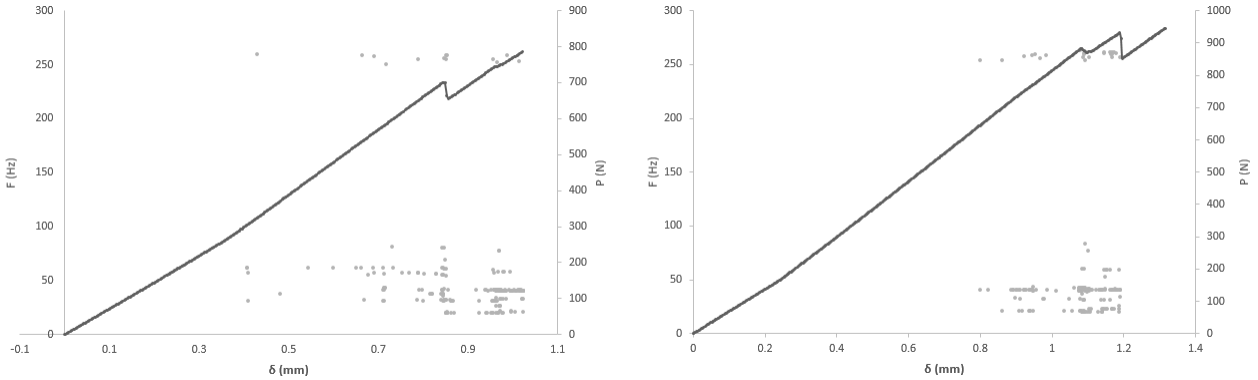

Figure A.2: Acoustic Emission: Specimen 2, fist test (left) and second test (right).

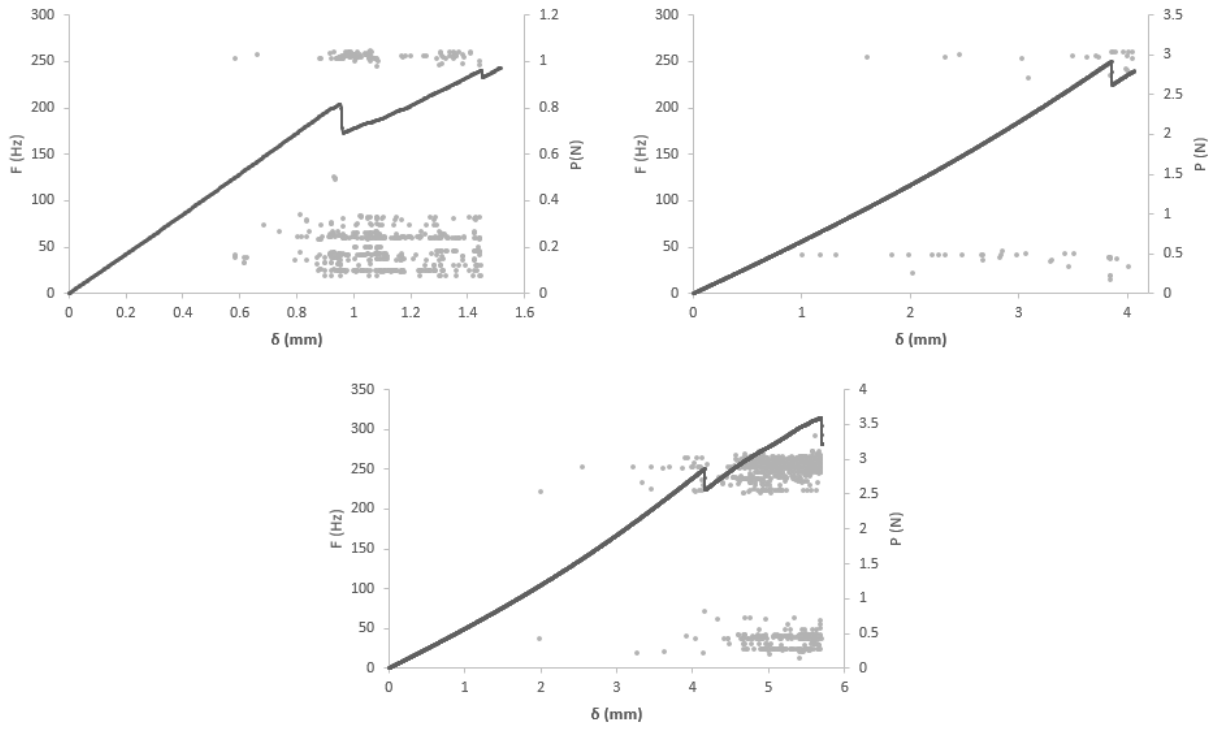

Figure A.3: Acoustic Emission: Specimen 5, first test (top left), second test (top right) and third test (bottom).

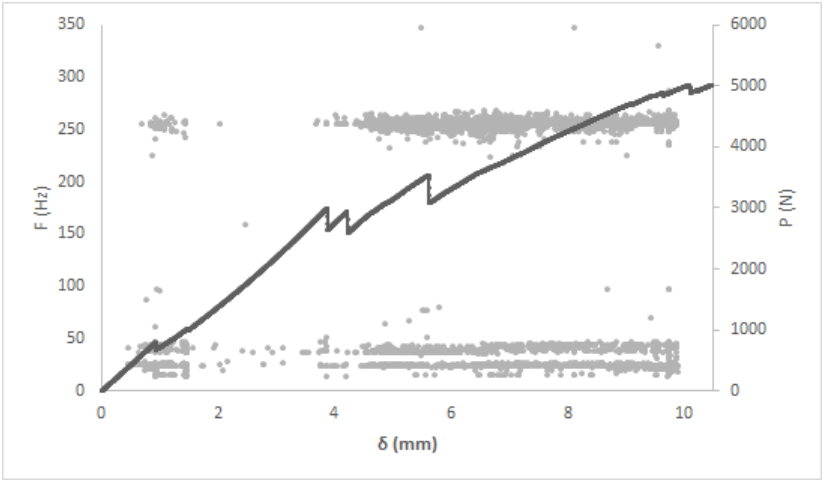

Figure A.4: Acoustic Emission: Specimen 6, 1st test (left) and 2nd test (right).

Appendix B

Ultrasonic inspection results (C-Scan)

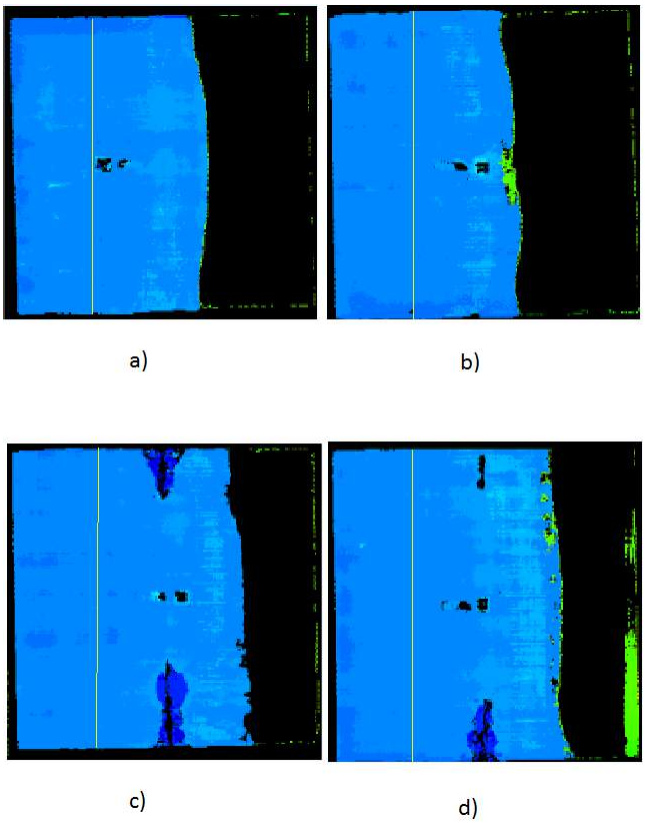

Figure B.1: C-Scans: a) Specimen 1(18%) b)Specimen 2(30%) c)Specimen 3(18%) d)Specimen 4(30%). Yellow line indicates initial crack position. Sky-blue represents 1.5mm depth and Sky-blue represents 1.8mm depth.

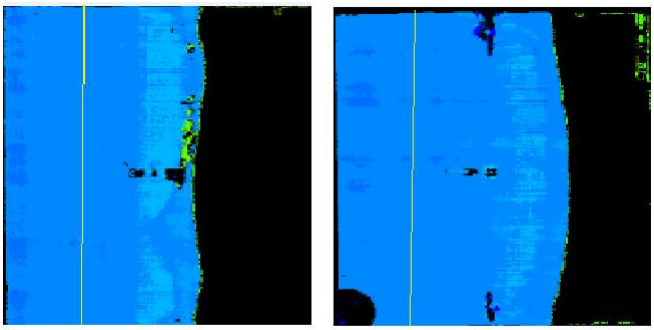

Figure B.2: C-Scans: e)Specimen 5(42%) f)Specimen 6(42%).Yellow line indicates initial crack position. Sky-blue represents 1.5mm depth and Sky-blue represents 1.8mm depth.

Appendix C

Ultrasonic inspection results (Dolphi Cam)

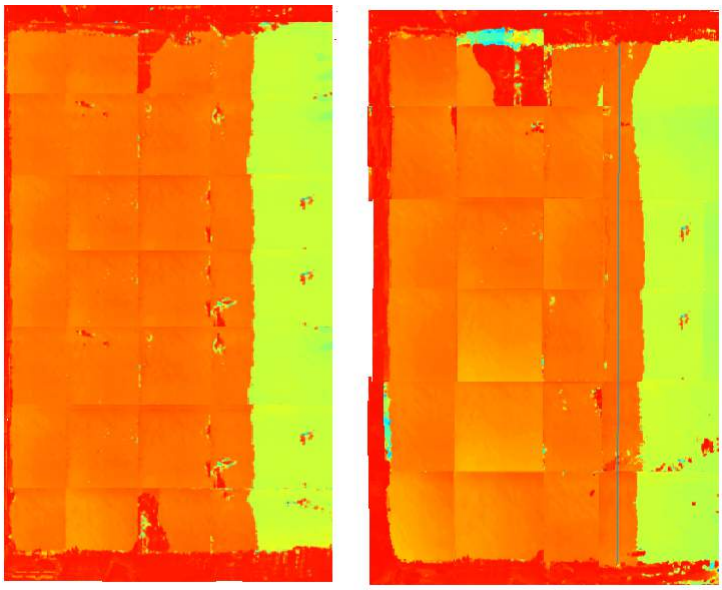

Figure C.1: Dolphi Cam: Specimen 4, 1st test (left) and 2nd test (right). Blue line indicates initial crack position. Orange represents 1.5mm depth and kiwi represents 3mm depth.

Appendix D

Fractography results

Firstly, the specimens that were going to be analysed both on the photomicroscope and by fractography were cut in two halfs, taking axis y as a symmetric axis. On one hand, the left half (L) was opened and then analysed fractographicly. On the other hand, three sections were obtained from the right part (R) of the specimen. The three sections were codified with 3 digits: the first represent the part of the specimen (right/left), the second denotes the specimen's number (1 to 6) and the last code illustrates the position within the specimen, from 1 to 3 (left to right). It is worth to highligh that all the specimens were orientatedly marked (faces and north orientation).

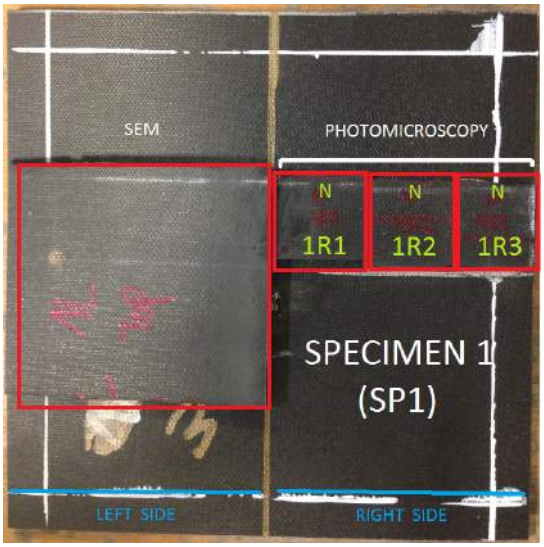

Figure D.1: Specimen's cut parts analysed by fractography/photomicroscopy. On top of a non-cutt specimen (S3) .

D.1 Optical Microscope

D.1.1 Specimen 1, 6PBP (18)

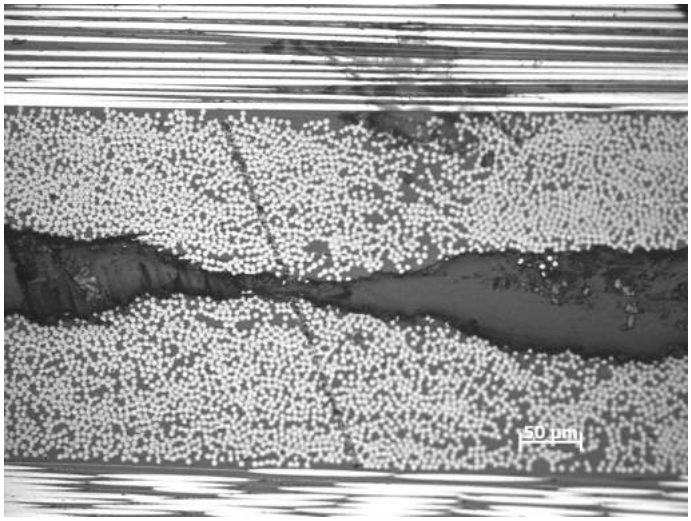

Figure D.2: 1R1 Photomicrograph of a 0°/0°interply at the insert edge.

Figure D.3: 1R2 Photomicrograph of a 0°/0°interply at the insert edge.

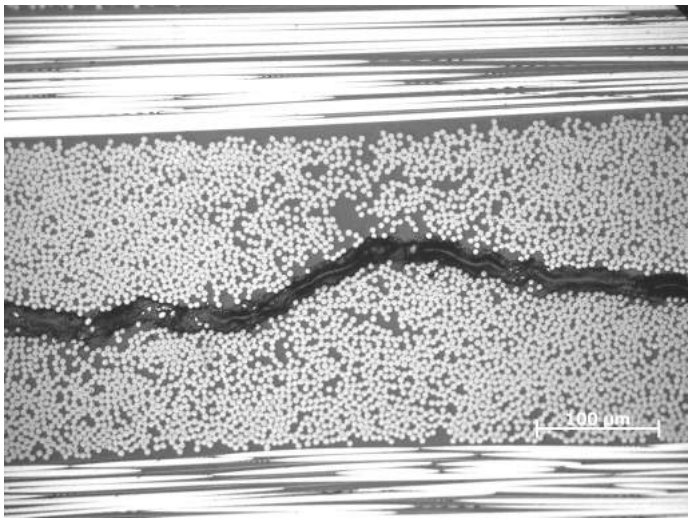

Figure D.4: 1R3 Photomicrograph of a 0°/0°interply at the insert edge.

D.1.2 Specimen 2, 6PBP (30)

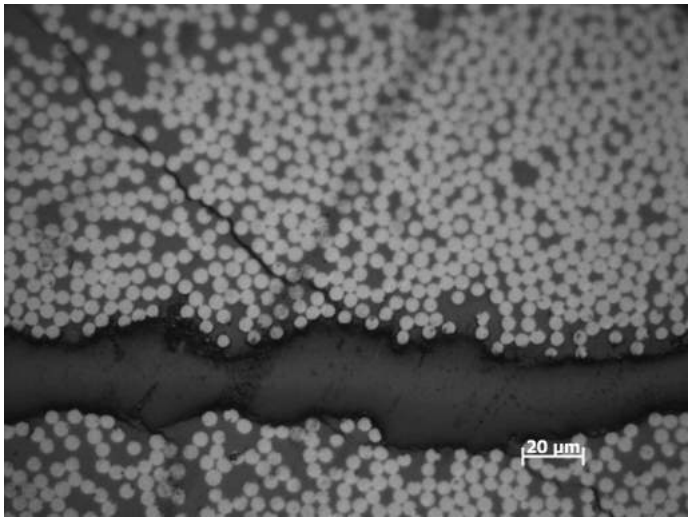

Figure D.5: 2R1 Photomicrograph of a 0°/0°interply at the insert edge.

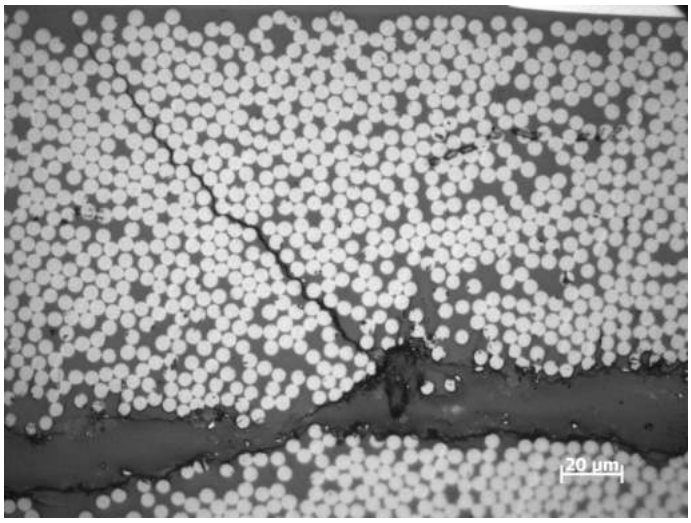

Figure D.6: 2R2 Photomicrograph of a 0°/0°interply at the insert edge.

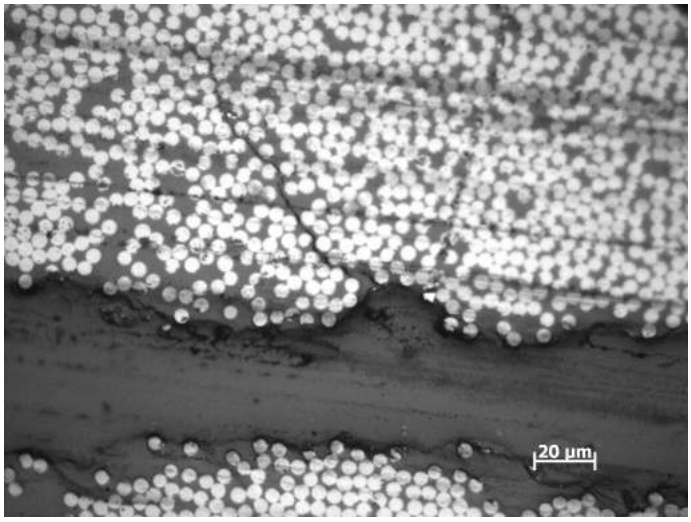

Figure D.7: 2R3 Photomicrograph of a 0°/0°interply at the insert edge.

D.1.3 Specimen 5, 6PBP (42)

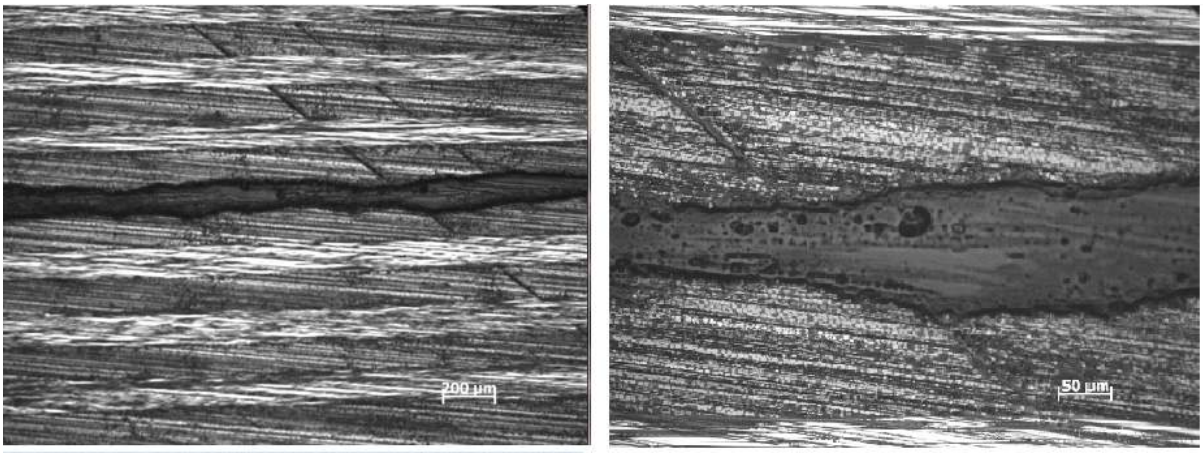

Figure D.8: 5R1 Photomicrograph of a 0°/0°interply at the insert edge.

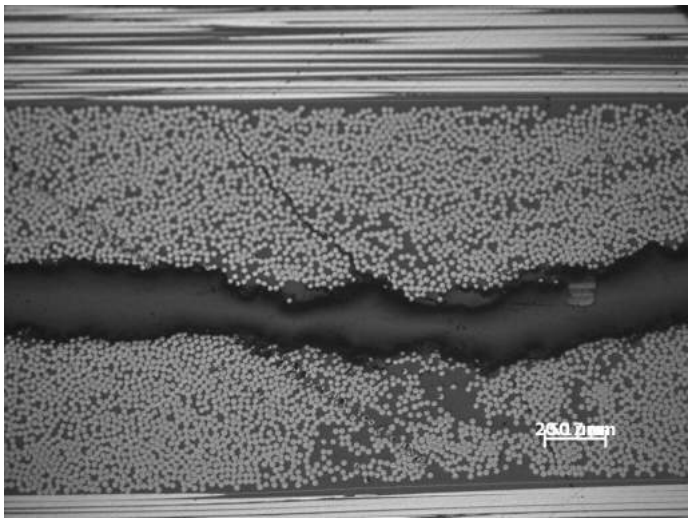

Figure D.9: 5R2 Photomicrograph of a 0°/0°interply at the insert edge.

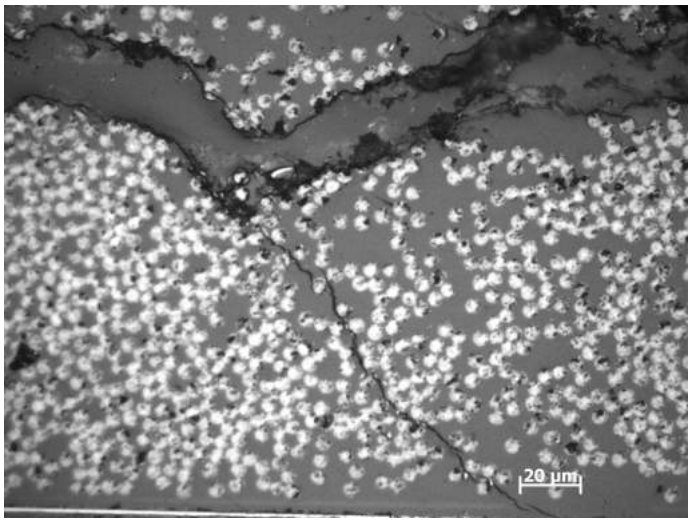

Figure D.10: 5R3 Photomicrograph of a 0°/0°interply at the insert edge.

D.2 Scan Electron Microscope (SEM)

An esquema of the procedure taken to analyse by fractography one section of the specimen is explained graphically is shown in the Fig.11.

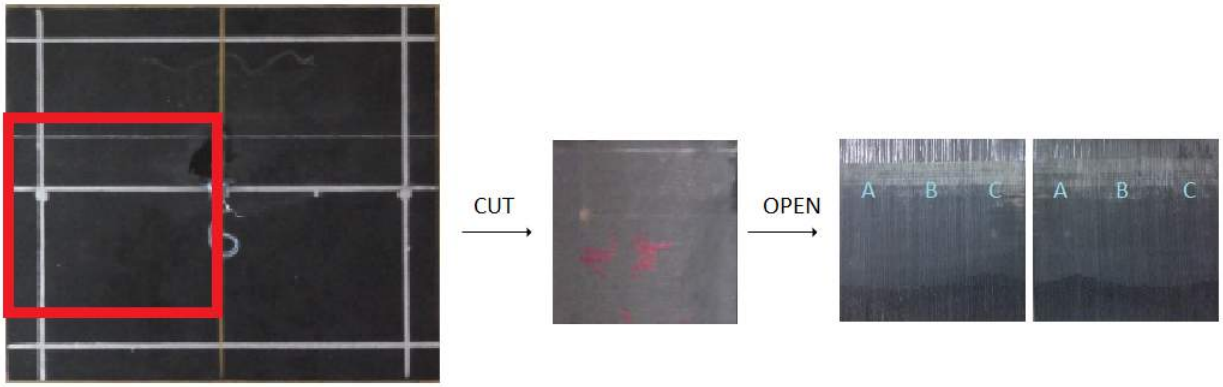

Figure D.11: Procedure to analyse by fractography one section of the specimen.

D.2.1 Specimen 1, 6PBP (18)

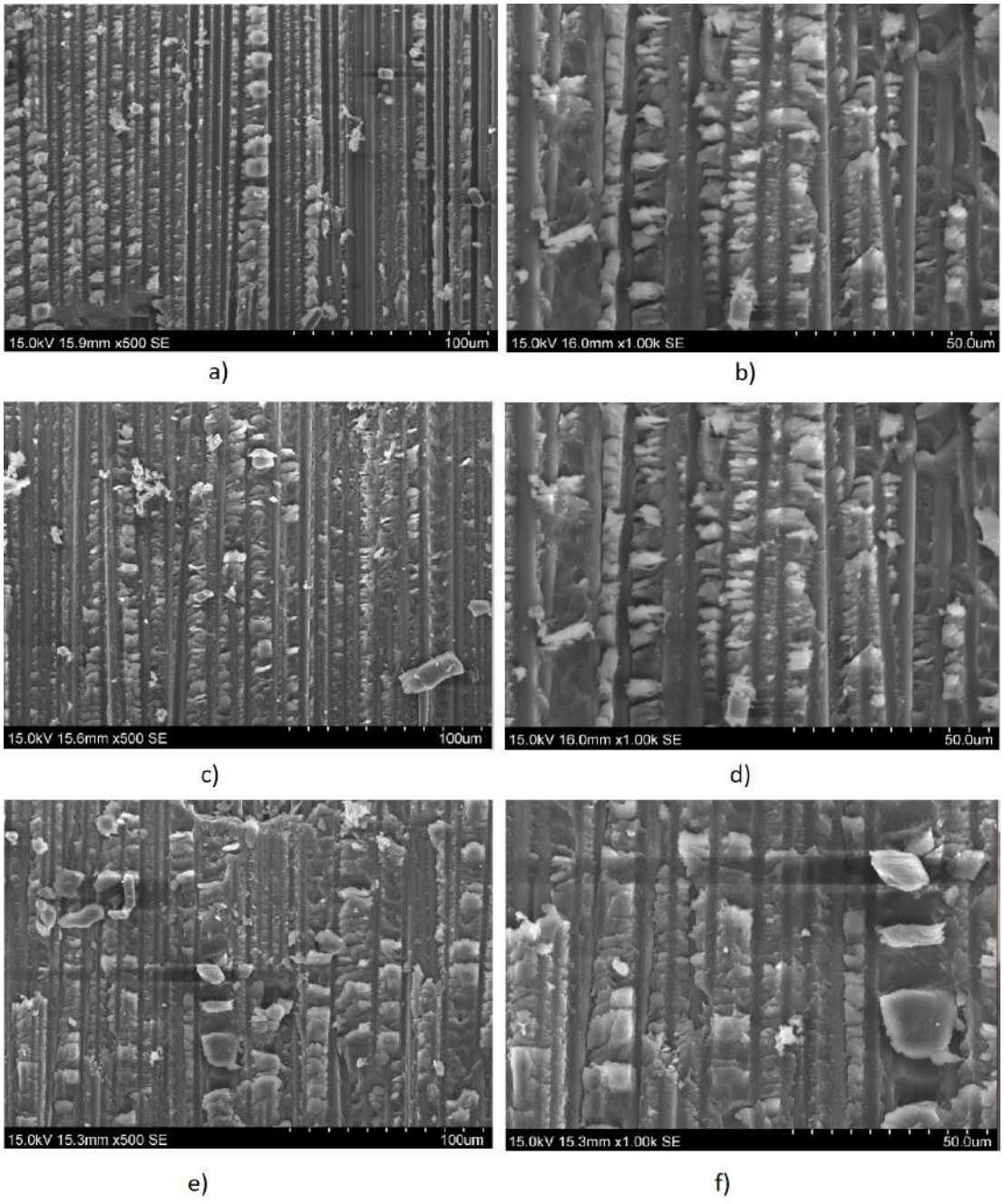

Figure D.12: Micrograph of S1 top face: a) b) Section A, c) d) Section B, e) f) Section C.

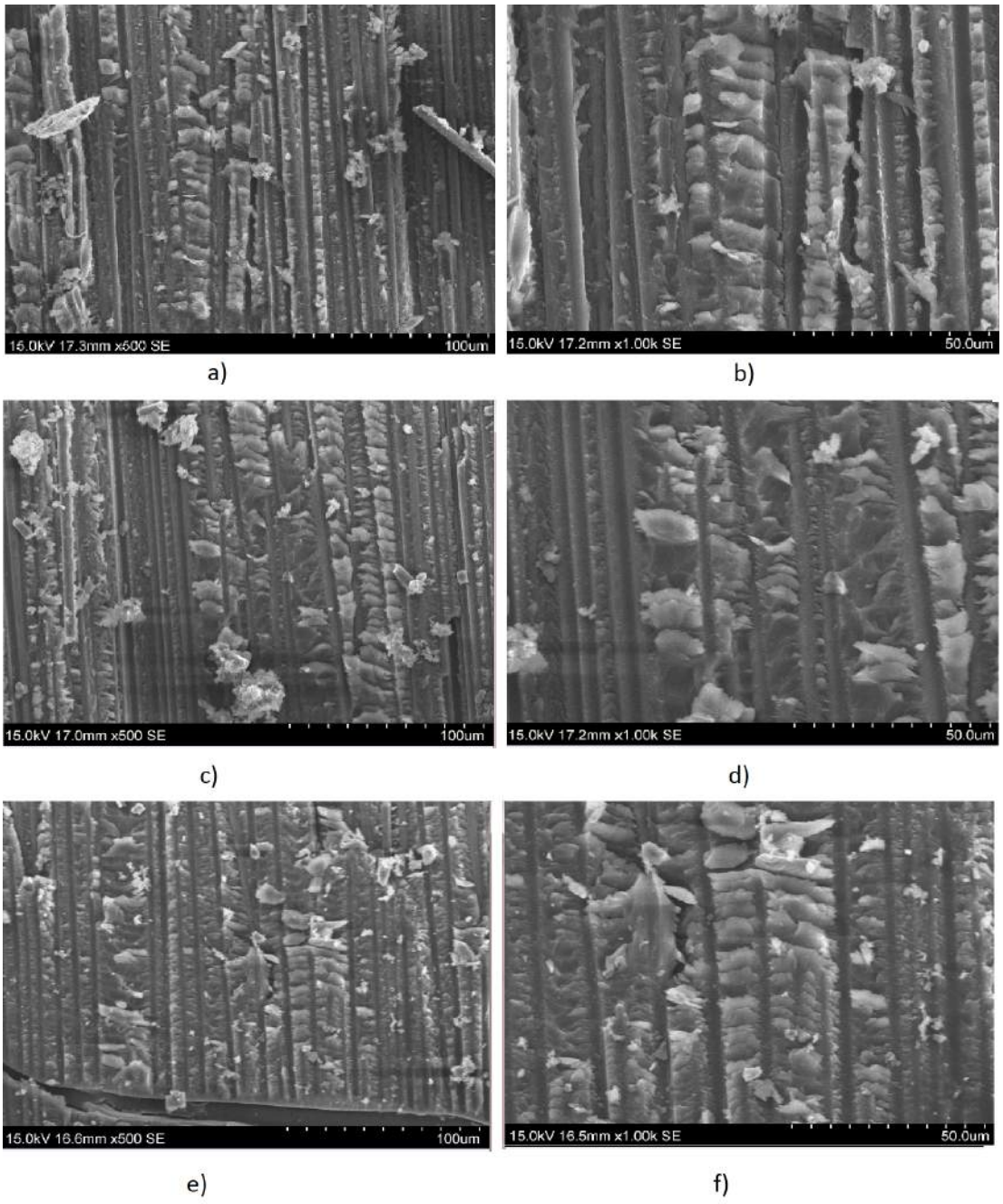

Figure D.13: Micrograph of S1 bottom face: a) b) Section A, c) d) Section B, e) f) Section C.

D.2.2 Specimen 2, 6PBP (30)

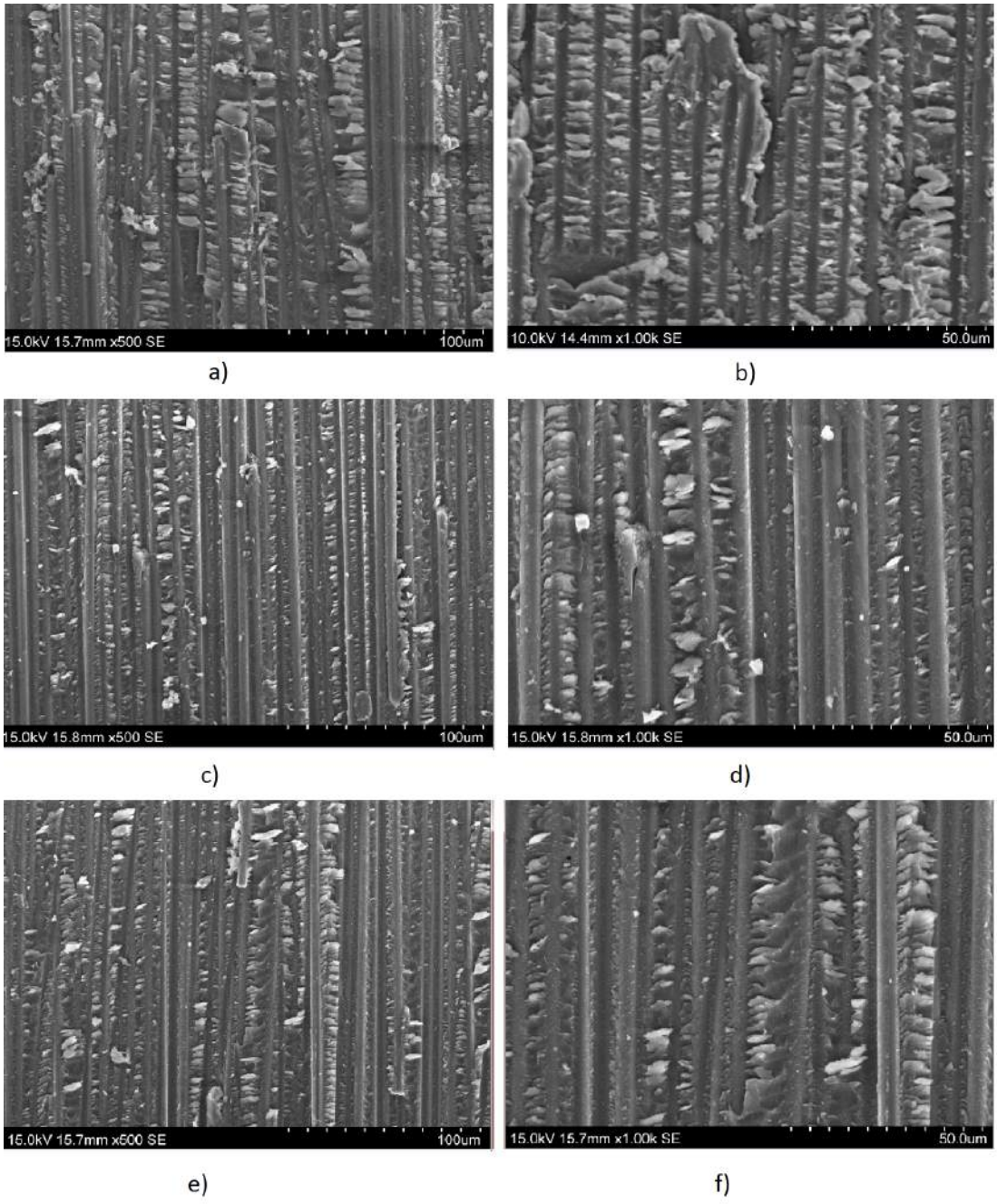

Figure D.14: Micrograph of S2 top face: a) b) Section A, c) d) Section B, e) f) Section C.

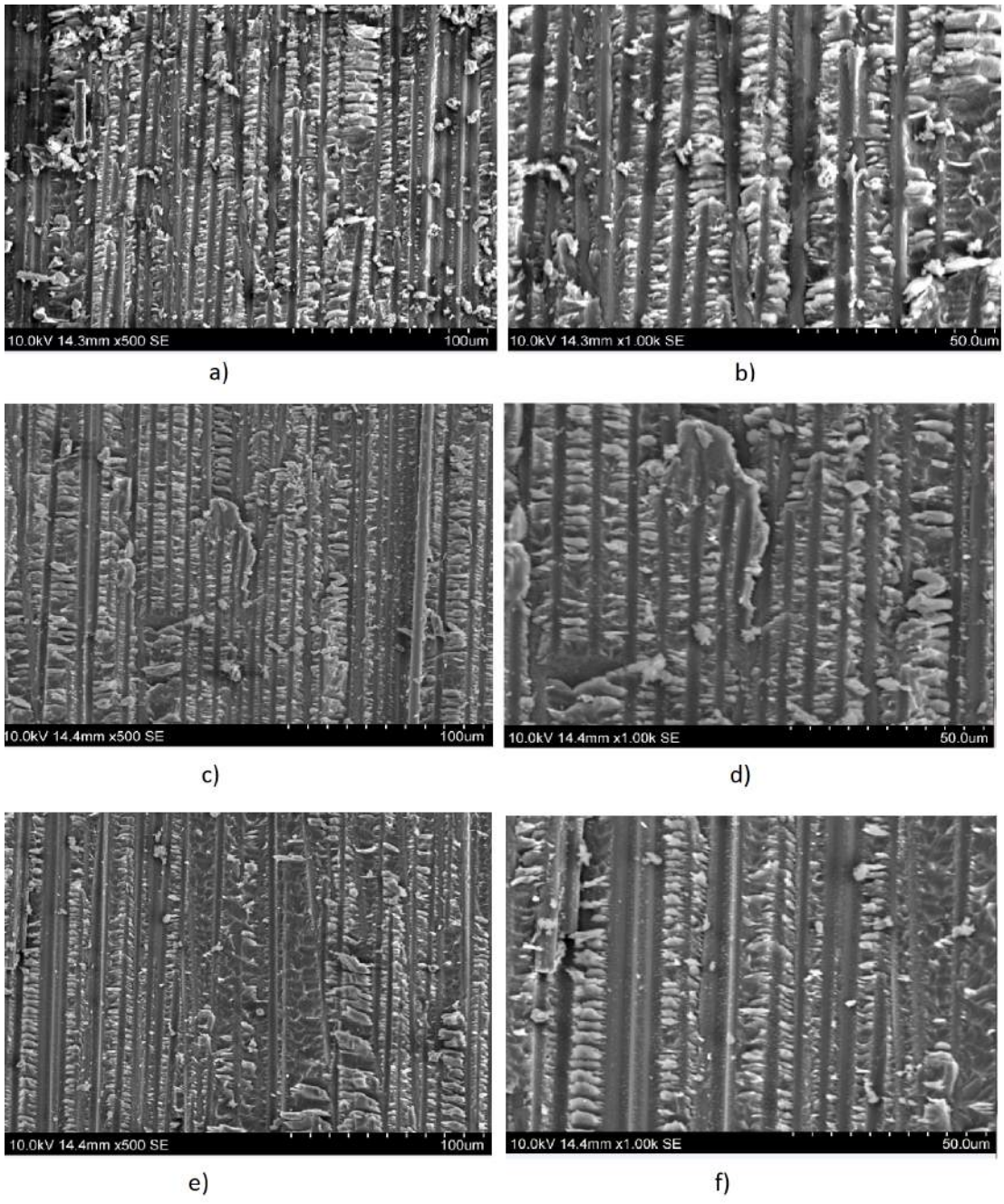

Figure D.15: Micrograph of S2 bottom face: a) b) Section A, c) d) Section B, e) f) Section C.

D.2.3 Specimen 5, 6PBP (42)

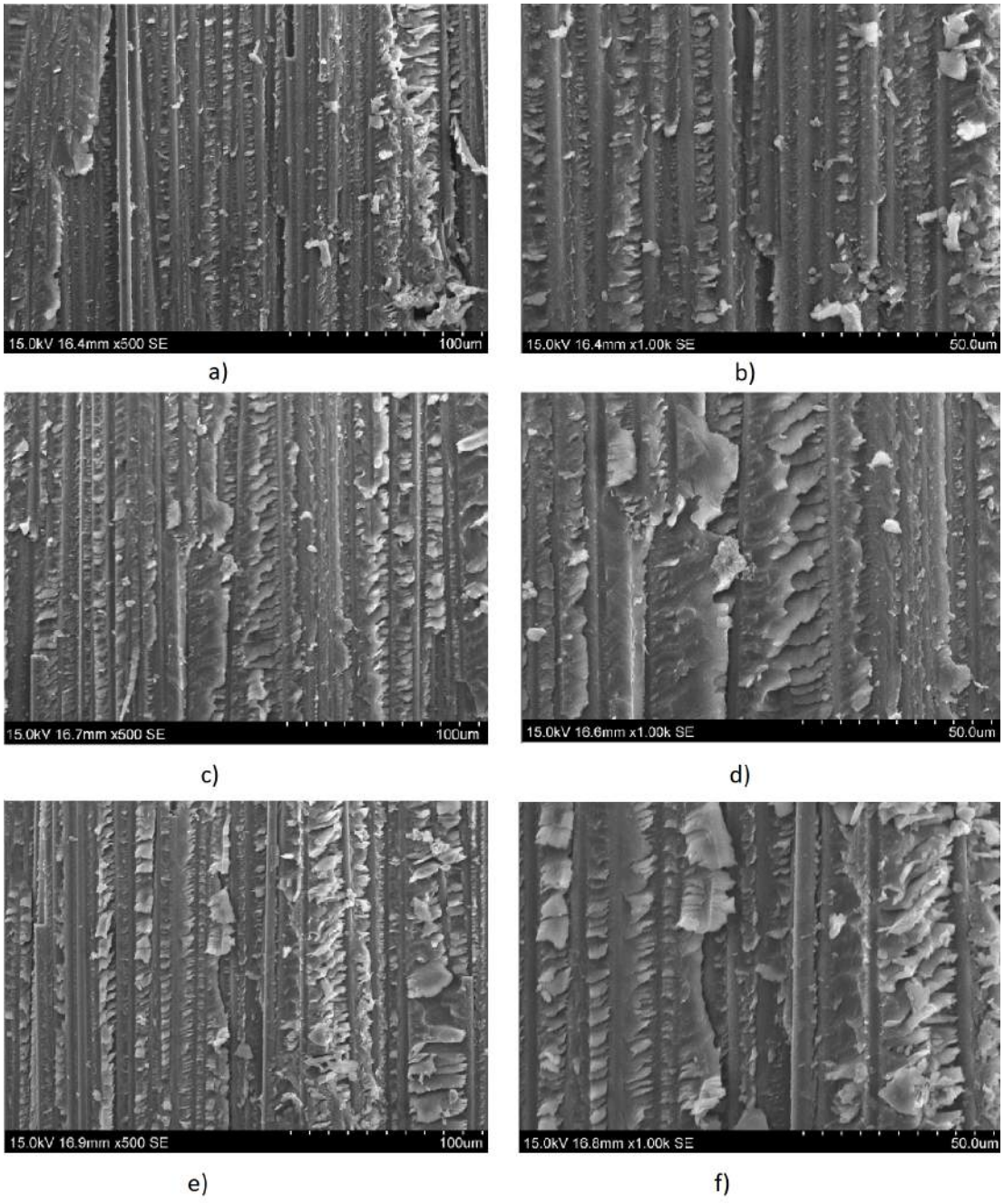

Figure D.16: Micrograph of S5 top face: a) b) Section A, c) d) Section B, e) f) Section C.

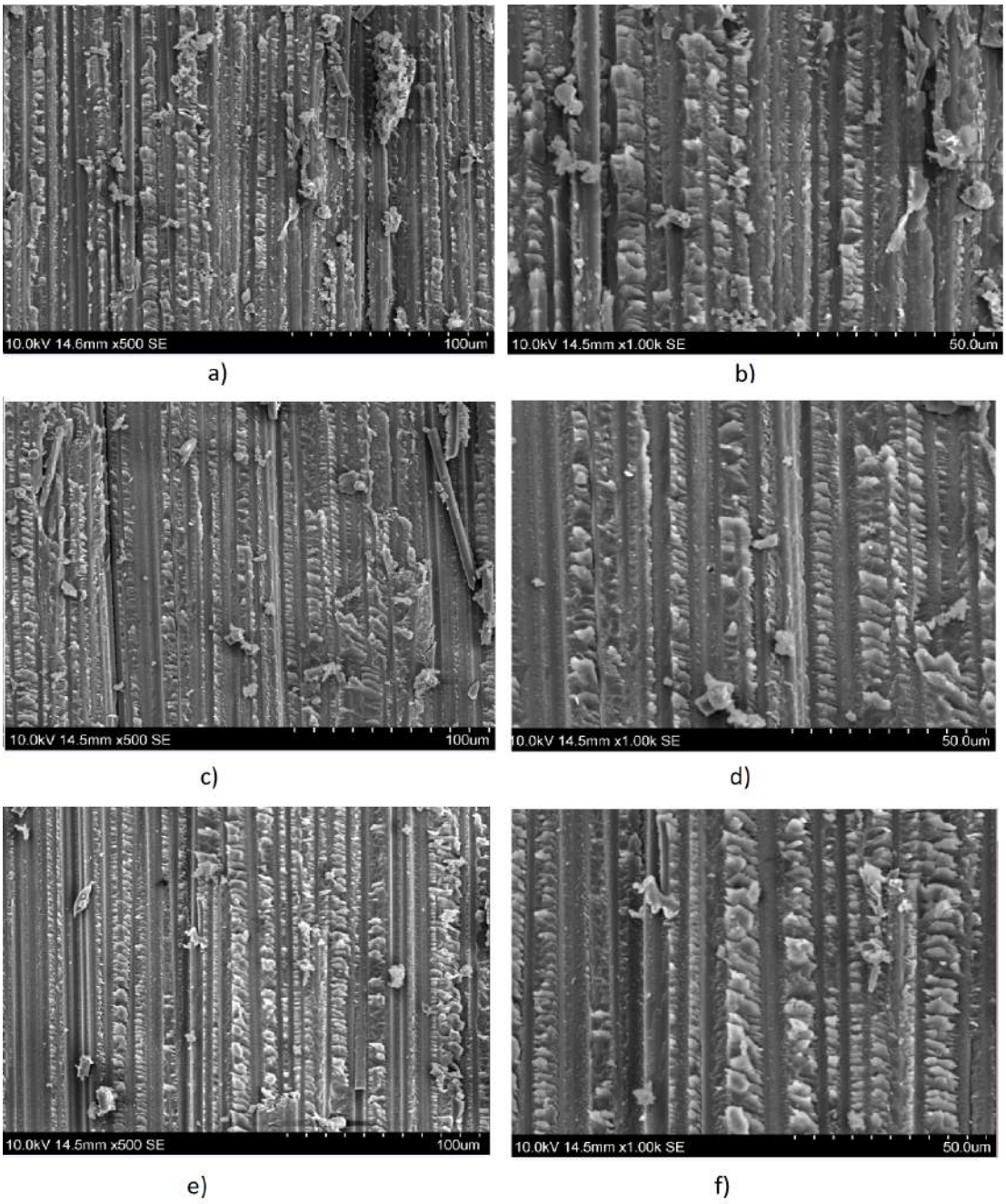

Figure D.17: Micrograph of S5 bottom face: a) b) Section A, c) d) Section B, e) f) Section C.

D.2.4 Masaya Miura, Yasuhide Shindo , Tomo Takeda, Fumio Narita [21]

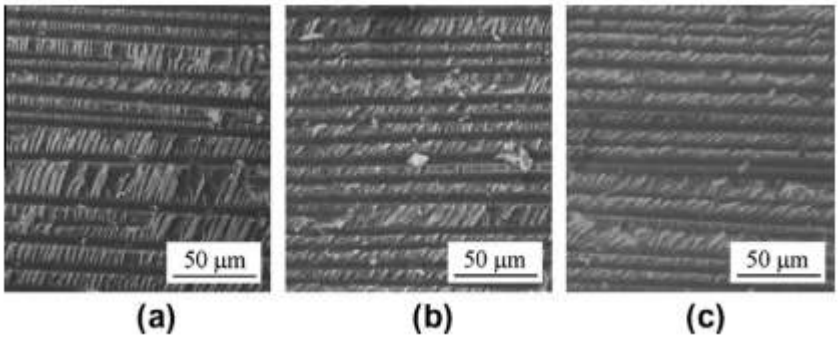

Figure D.18: Fracture surfaces at 4 K for (a) GIII/GT = 0.30, (b) GIII/GT = 0.56 and (c) GIII/GT = 0.75 (delamination growth from left to right) [21].

Appendix E

6PBP Engineering Drawings

A new fixtures had been designed from scratch taking advantadge from some that had been already manufactured. On one hand, there are those that had been re-utilised which are part B and part F. On the other hand, part A, part C, part D and part E had been designed taking into account the adaptability in the parts that were already done. Find attached both the global assembly where all parts could be identified and the engineering drawings of each part.

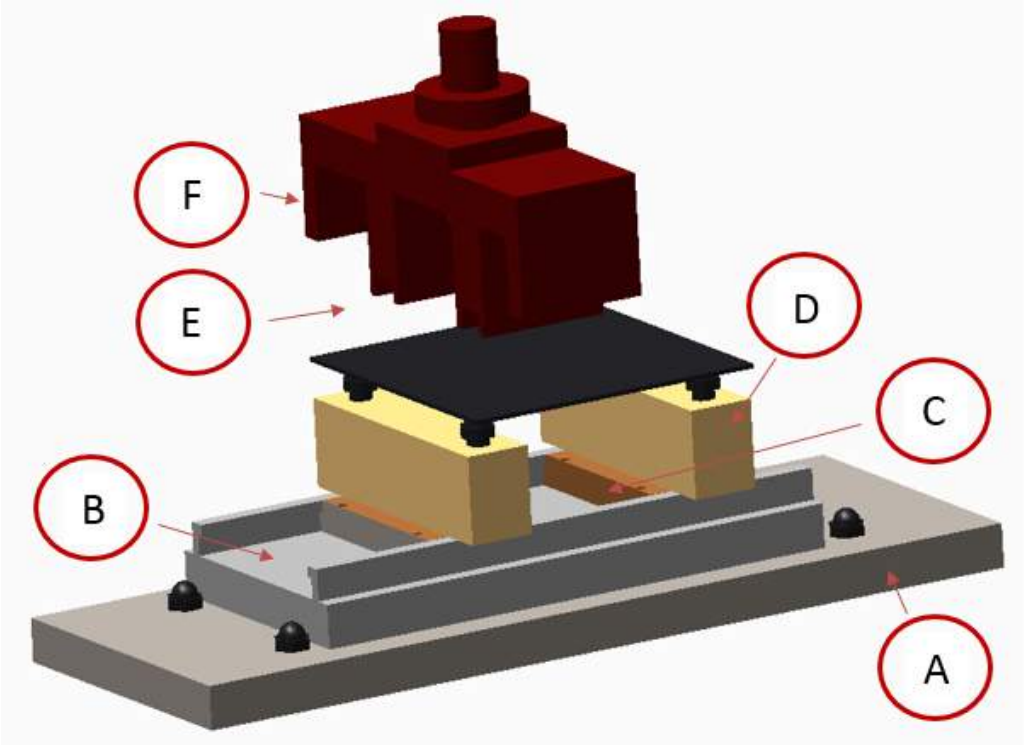

Figure E.1: Six-point bending point engineering drawing assembly

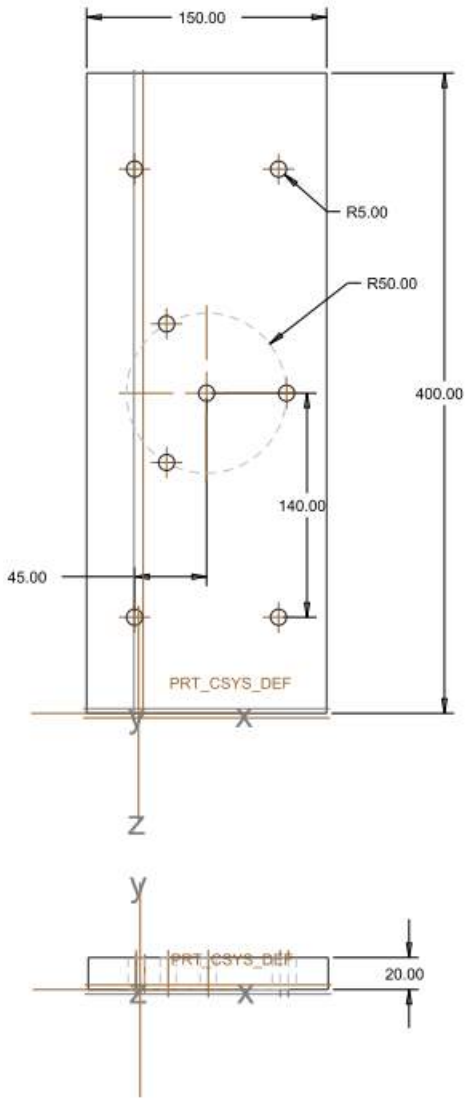

Figure E.2: Engineering drawings Part A

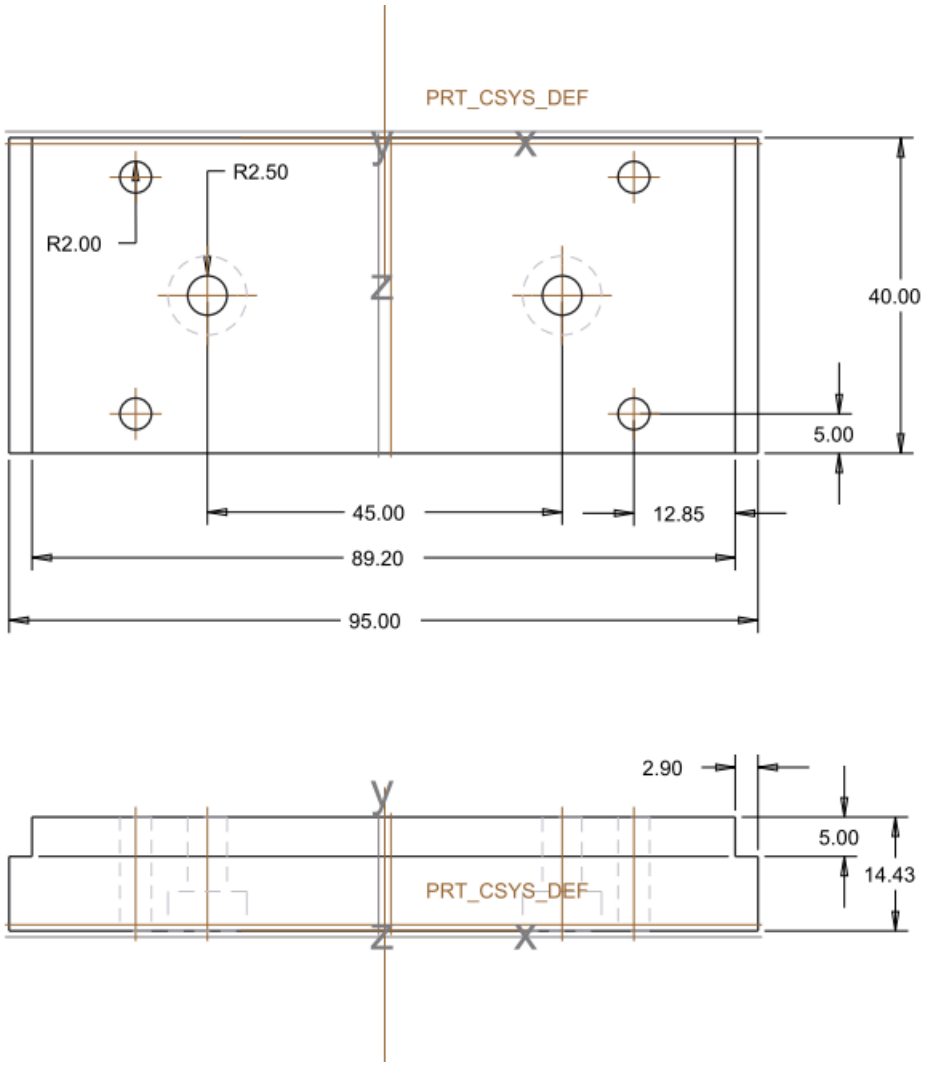

Figure E.3: Engineering drawings Part C

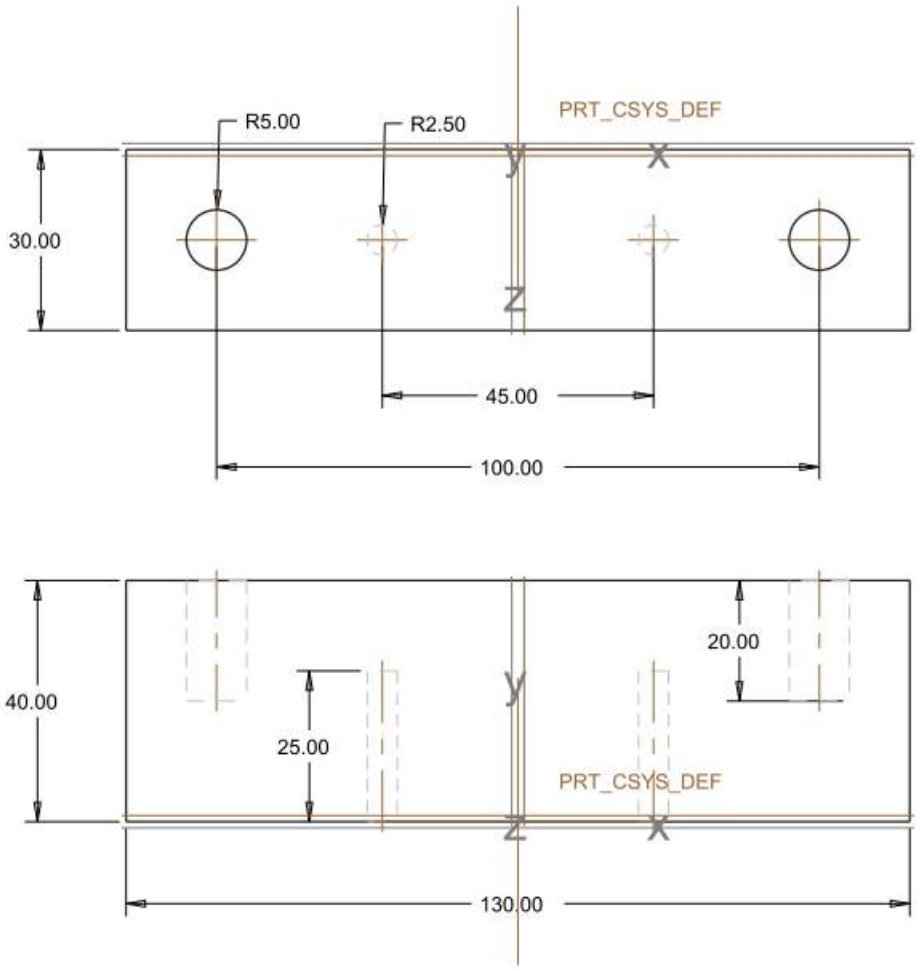

Figure E.4: Engineering drawings Part D

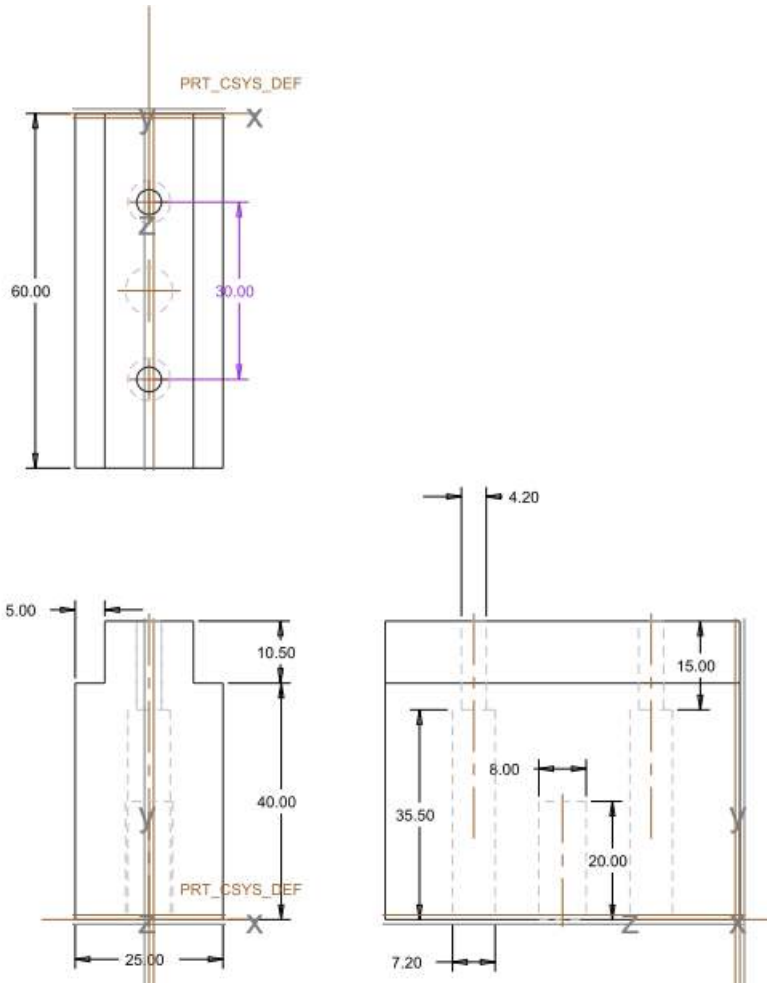

Figure E.5: Engineering drawings Part E

Appendix F

FEA Tailor-made tutorial (Abaqus 6.14-1)

Create a part and the skecht by creating the rectangle and then insert the depth of the extrusion:

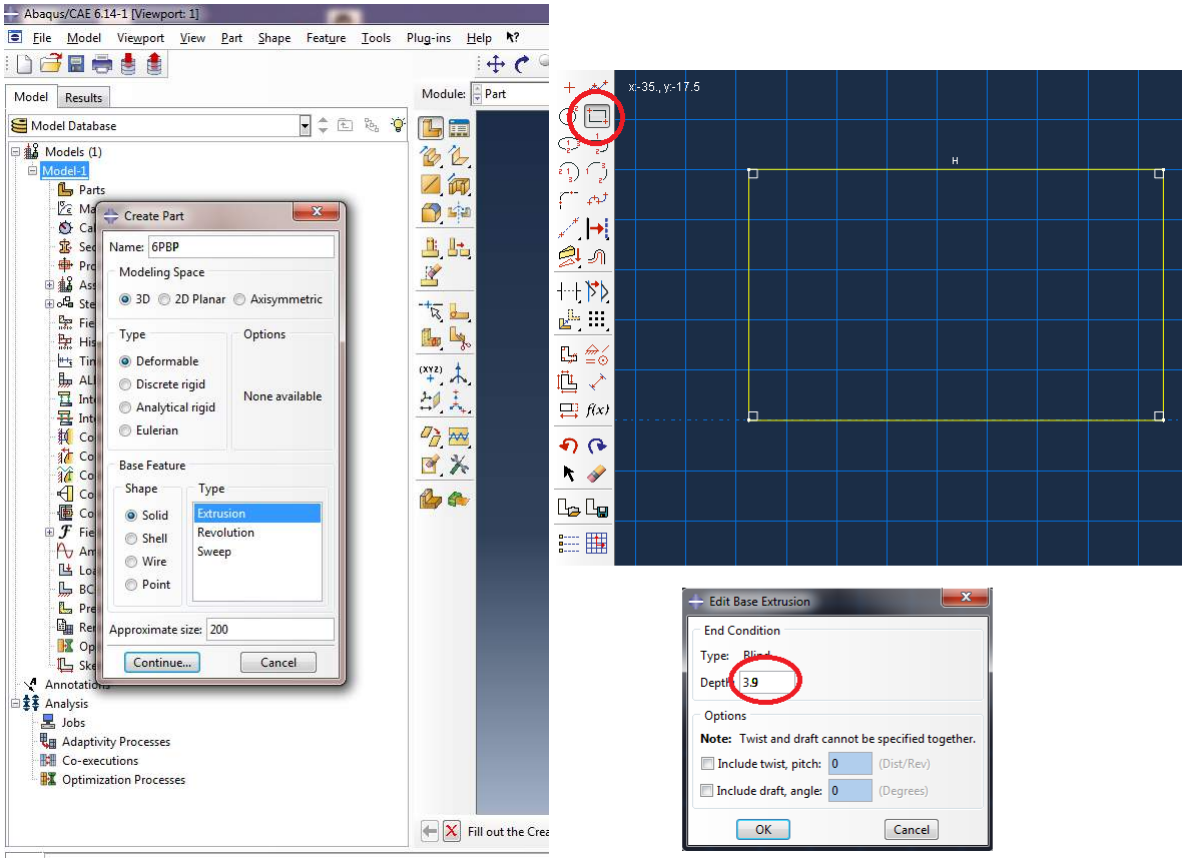

Create the laminates by creating partition. Reference points should be determined before.

Then, click on the 'Partition Cell: Use Datum Plane' bottom and follow the pop messages.

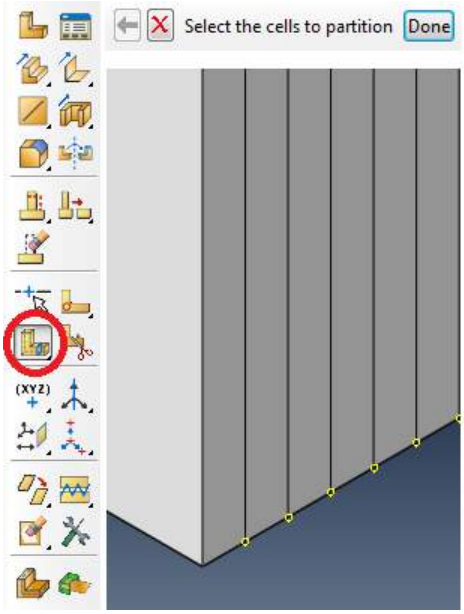

As the composite is manufactured within two halfs and a starter delamination between them, these two halfs must be designed independently. To get the second half and save some time, the half that has been already done could be mirrored.

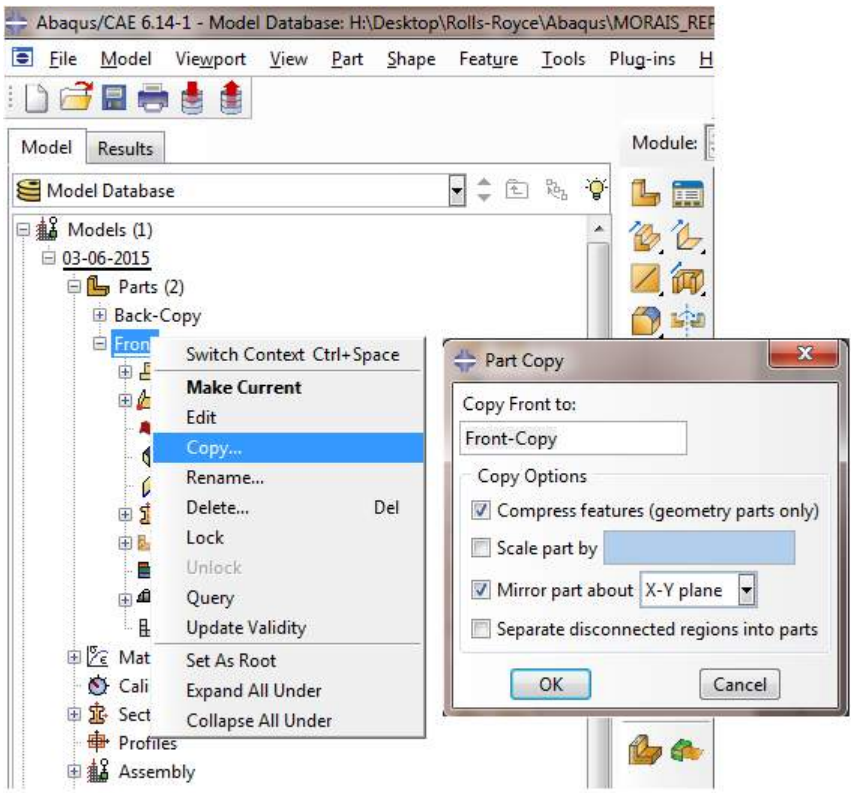

Once the two halfs are done, the material must be created and then assigned to a section. So, the actions that must be followed in order are: a)Create the material, b)Create a section, c)Assign section:

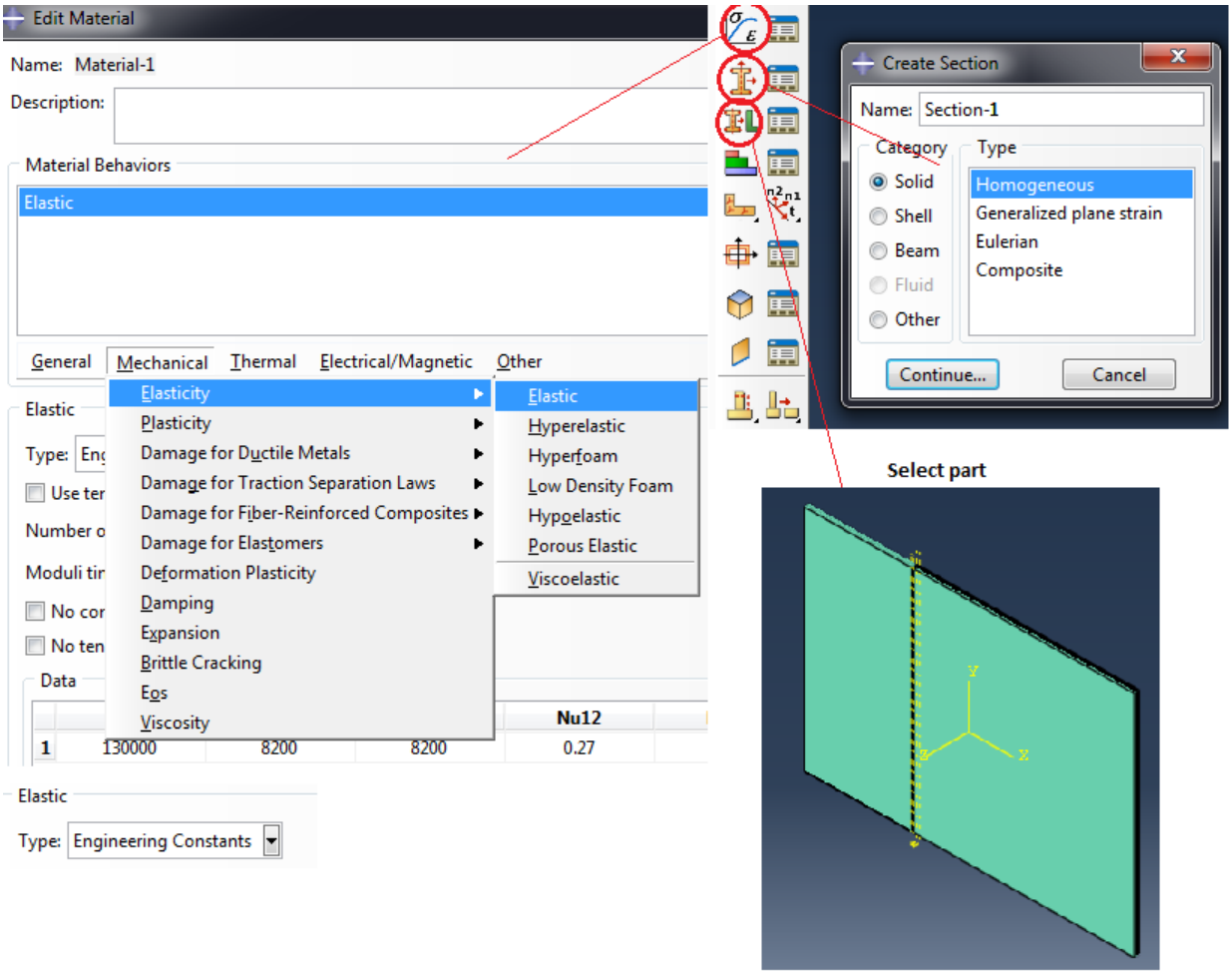

d)Create datum CSYS: 3 Points

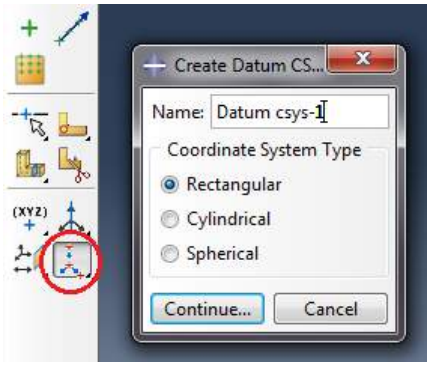

And finally e) Assign an orientation to each ply (based on the stacking sequence that had previously designed).

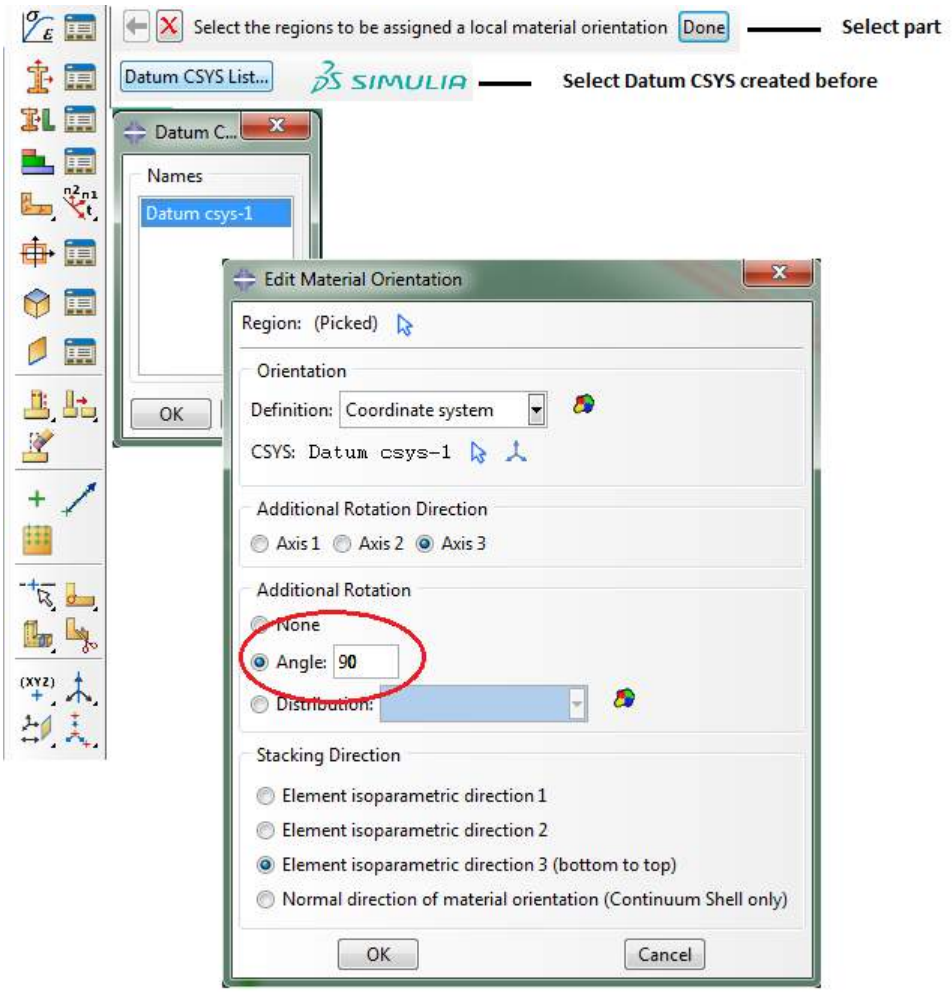

Create a step:

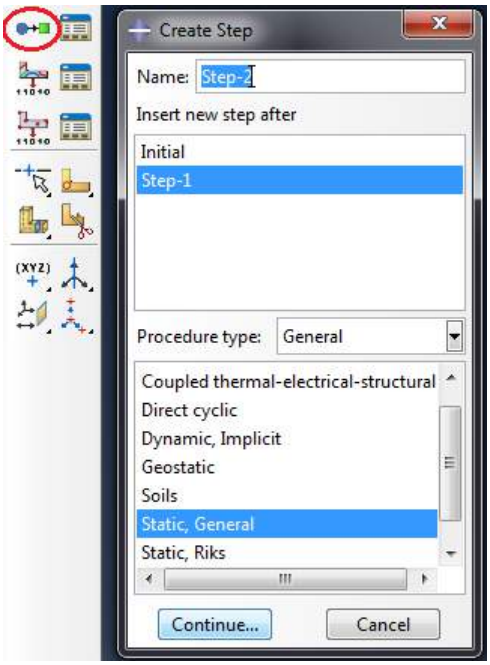

Create the assembly:

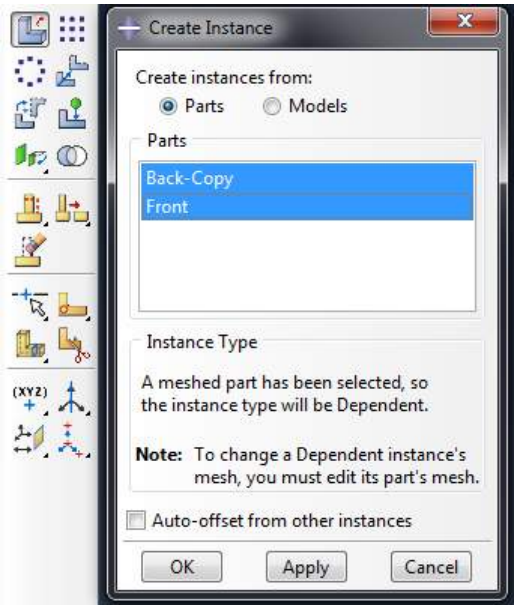

Mesh individually both halfs. Seed first all the edges.

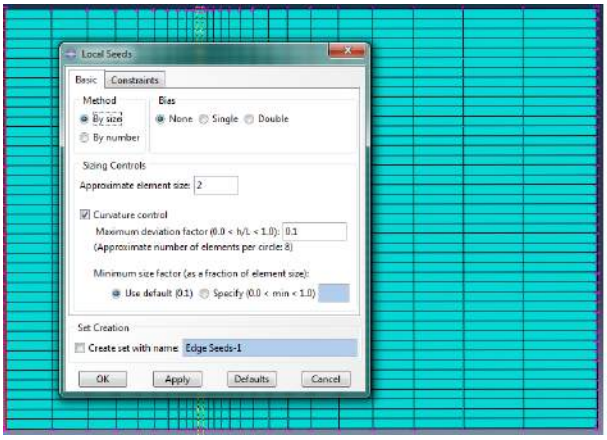

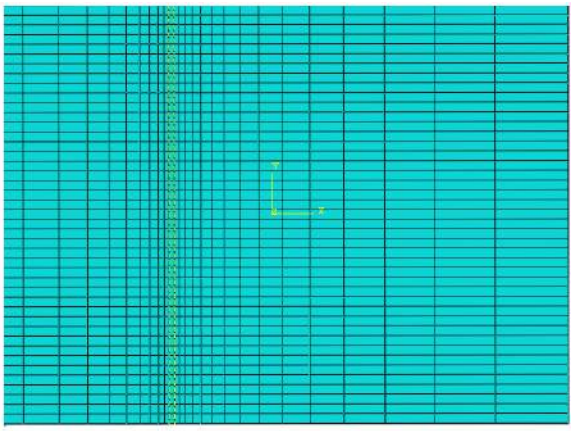

Create 4 sets: a) To locate the load, b) To locate the supports, c) To select the bonded nodes that would need to be selected when defining the interaction, d) To determine the symmetry.

Middplane bonded nodes

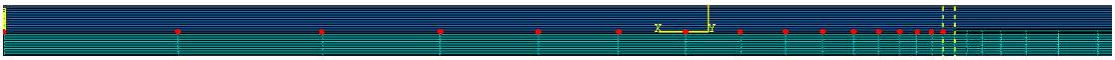

Symmetry nodes

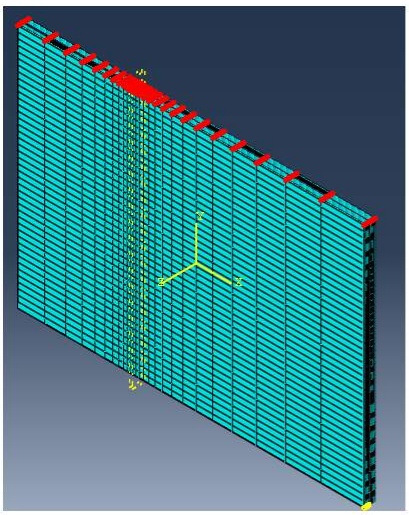

Load and support nodes

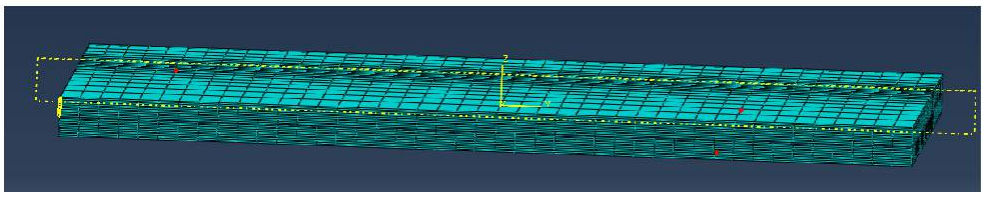

Create an interaction. Determine interaction properties:

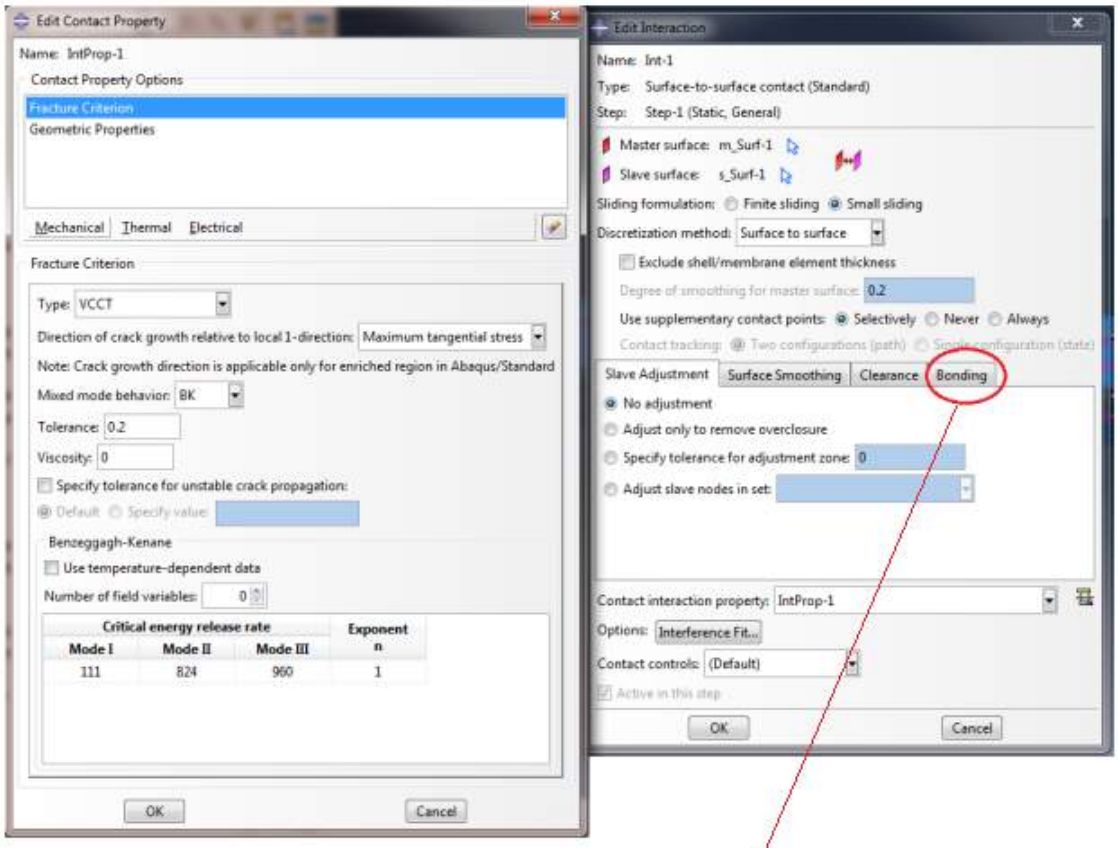

Note: Contact bonding is enabled in the cohesive behavior option of the contact interaction property. This set can also be used to specify the initially bonded nodes of the slave surface in debond using VCCT crack.

Determine the appropiated bondary conditions. This project consist of a six-point bending plate so there will be 3 BC and 1 extra BC due to the symmetry.

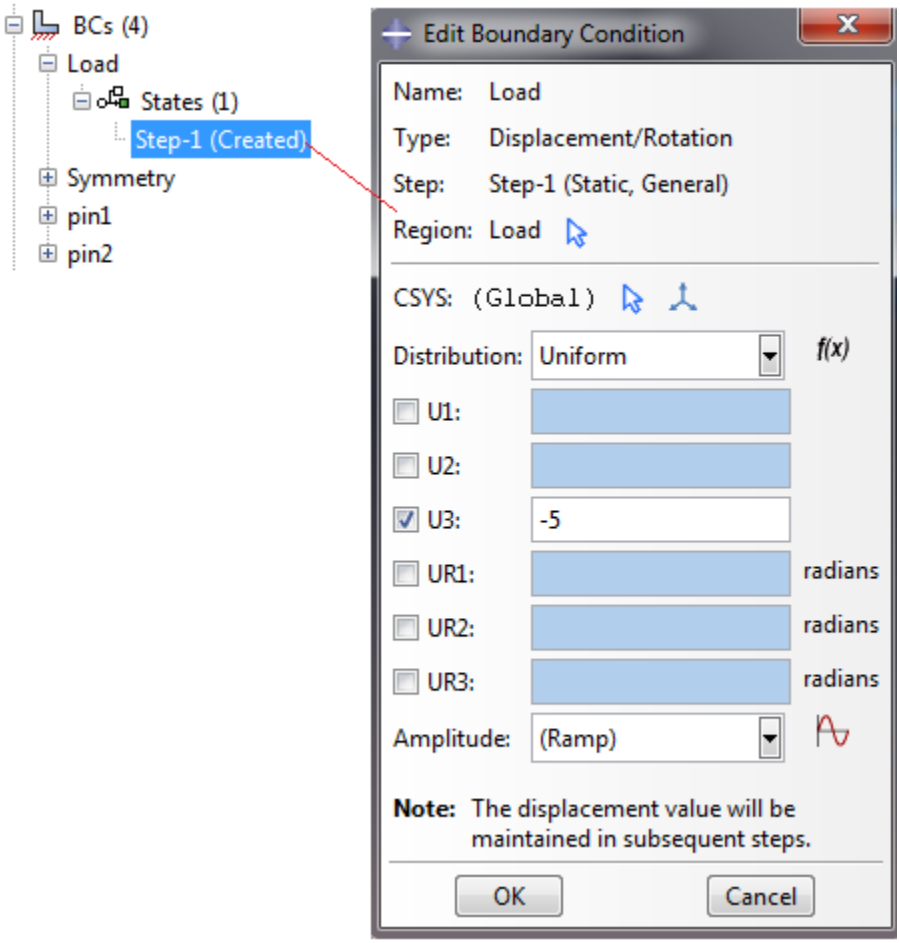

Define VCCT properties:

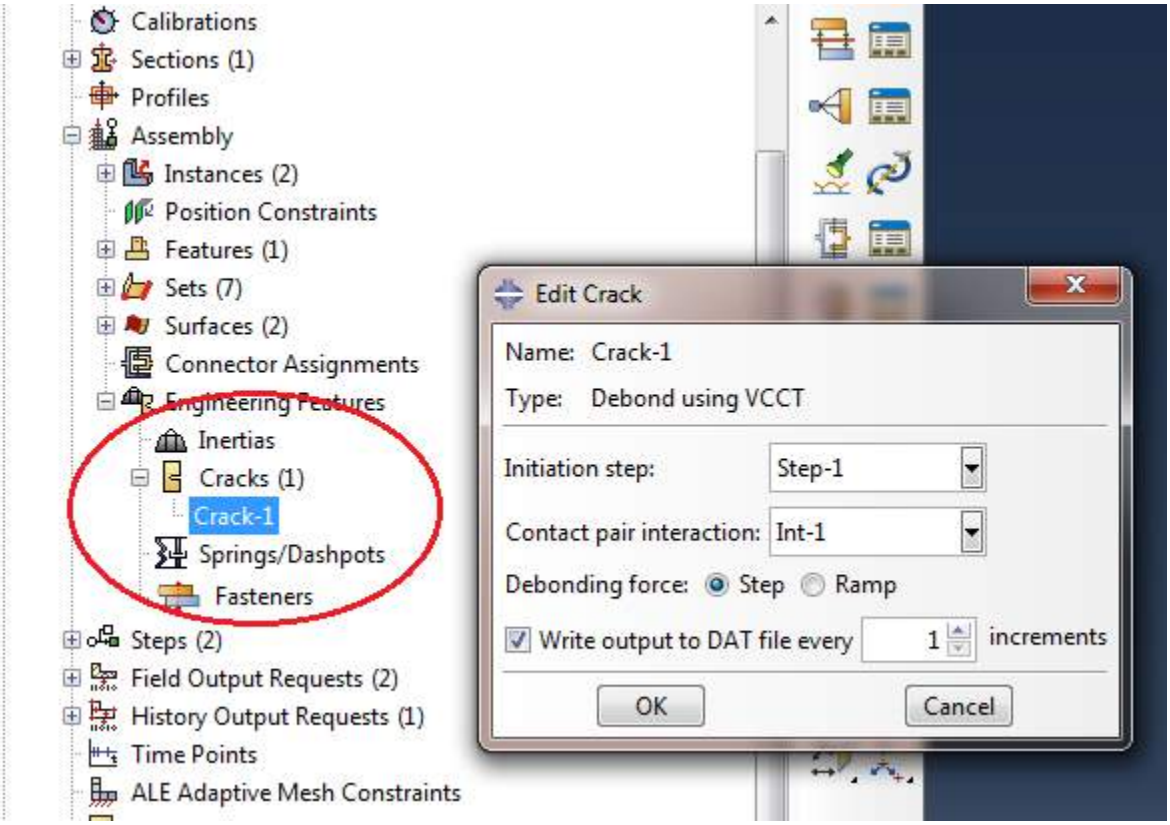

Define the output data to be analysed:

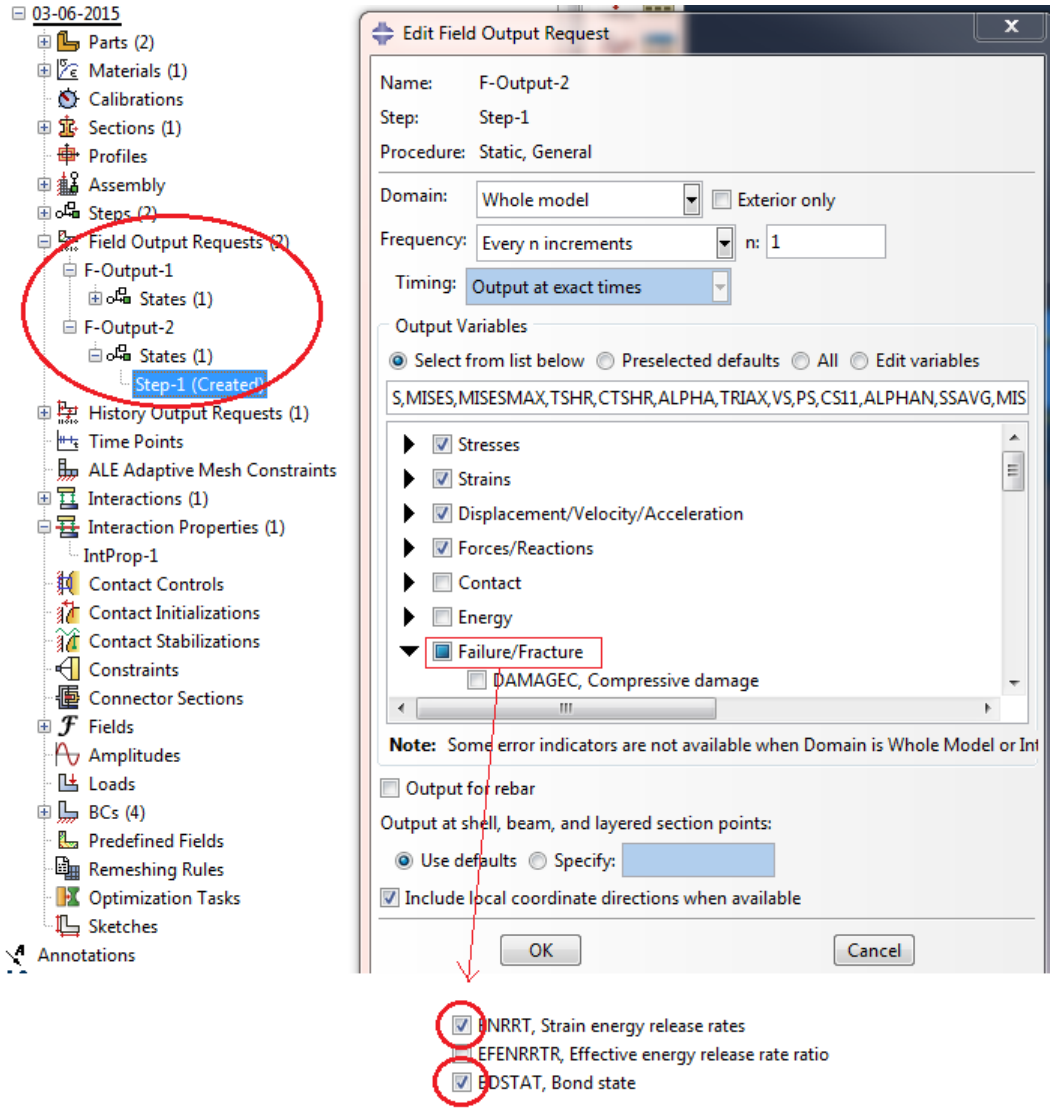

Create a job:

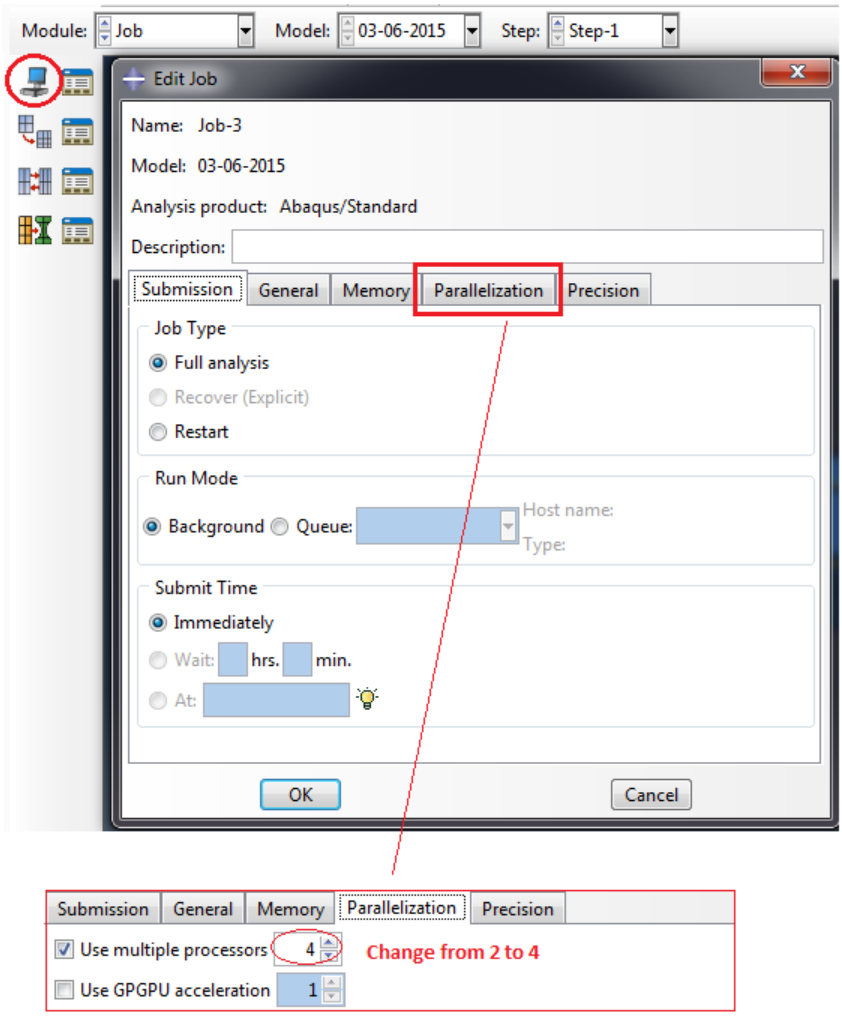
Module: Job
Model: 03-06-2015
Step: Step-1
Edit Job
Name: Job-3
Model: 03-06-2015
Analysis product: Abaqus/Standard
Description:
Submission
General
Memory
Parallelization
Precision
Job Type
Full analysis
Recover (Explicit)
Restart
Run Mode
Background
Queue:
Host name:
Type:
Submit Time
Immediately
Wait:
hrs.
min.
At:
OK
Cancel
Submission
General
Memory
Parallelization
Precision
Use multiple processors
4
Change from 2 to 4
Use GPGPU acceleration
1

Appendix G

Material properties

IM7/8552	Property	Room temperature
Ply longitudinal modulus	E_x	165 GPa
Ply transverse modulus	E_y	9.4 GPa
In-plane shear modulus	G_{xy}	4500 MPa
Out-of-plane shear modulus	G_{xz}	4290 MPa
Out-of-plane shear modulus	G_{yz}	3190 MPa
Poisson's ratio	ν	0.3
Ply longitudinal tensile strength	X_T	2600 MPa
Ply longitudinal compressive strength	X_C	1500 MPa
Ply transverse tensile strength	Y_T	60 MPa
Ply transverse compressive strength	Y_C	290 MPa
Ply shear strength	S	90 MPa
Interlaminar shear strength	ξ_{xy}	117 MPa
Interlaminar shear strength	ξ_{xz}	38 MPa
Critical strain energy release rate for mode I *	G_{IC}	0.235 J/m^2
Critical strain energy release rate for mode II *	G_{IIC}	0.768 J/m^2
Coefficient of thermal expansion [185]	α_x	25 x 10^{-9} °C^{-1}
Coefficient of thermal expansion [186]	$\alpha_y=\alpha_z$	22.5 x 10^{-6} °C^{-1}
Ply thickness	t	0.250 mm
Density *	ρ	1 x 10^{-9} Kg/mm^3

Bibliography

[1] Ireman, Tomas (2001), "*Efficient Design and Verification of Composite Structures",* European Community under the Industrial & Materials Technologies, Program (Brite-Euram III), Project BE97-4359.

[2] Orders and Deliveries, The Airbus Company Market Orders, Airbus S.A.

[3] Orders and Deliveries, Commercial, The Boeing Company.

[4] L. Ilcewicz at 11/10/09 Montana State Univ. Seminar.

[5] Case in point: Complete Case Interview Preparation, Marc P. Cosentino.

[6] Optimisation and Simulation, Second Cycle Curricular; Industrial Engineering at ETSEIB, UPC.

[7] Quantitative Management Methods, Second Cycle Curricular; Industrial Engineering at ETSEIB, UPC.

[8] Operations Management, Second Cycle Curricular; Industrial Engineering at ETSEIB, UPC.

[9] Canturri C., E. S. Greenhalgh and S. T. Pinho. 2014. "The relationship between mixed-mode II/III delamination and delamination migration in composite laminates," Composites Sci, In press.

[10] de Morais A. B., A. B. Pereira. 2008. "Mixed mode II + III interlaminar fracture of carbon/epoxy laminates," Composites Sci.Technol., 68(9):2022-2027.

[11] Crewa JH, Reeder JR. Mixed-mode bending apparatus for delamination testing. NASA Technical Memorandum 1988;100662.

[12] Lee SM. An Edge Crack Torsion Method for Mode-III Delamination Fracture Testing. Journal of Composites Technology & Research 1993;15(3) 193-201.

[13] Pereira AB, de Morais AB. Mixed mode I-III interlaminar fracture of carbon/epoxy laminates. Composite Part A: Applied Science and Manufacturing 2009;40(4) 518-523.

[14] Brunner AJ, Fluer P. Prospects in fracture mechanics of "engineering" laminates, Eng Fract Mech 2005;72:899-908.

[15] Brunner AJ, Blackman BRK, Davies P. A status report on delamination resistance testing of polymer-matrix composites. Eng Fract Mech 2008; 75; 2779-94

[16] Li J, See SM, Lee EW, O'Brien TK. Evaluation of the edge crack torsion (ECT) test for mode III interlaminar fracture toughness of laminated composites. J Compos Technol Res 1997; 19:174-83.

[17] Ratcliffe JG. Characterization of the edge crack torsion (ECT) test for mode III fracture toughness measurement of laminated composites. NASA/TM-2004-213269.

[18] Reeder JR. Refinements to the mix-mode bending test for delamination toughness. J Compos Technol Res 2003; 25:191-5.

[19] ASTM D 6671-04. Standart test method for mixed mode I-mode II interlaminar fracture thoughness of unidirectional fiber-reinforced polymer matrix composites.

[20] Szekrenyes A. Delamination fracture analysis in the GII-GIII plane using prestressed transparent composite beams. Int J Solid Struct 2007;44:3359-78.

[21] Interlaminar fracture characterization of woven glass/epoxy composites under mixed-mode II/III loading conditions at cryogenic temperatures; Masaya Miura, Yasuhide Shindo , Tomo Takeda, Fumio Narita.

[22] Wu, E. M., and R. C. Reuter Jr., "Crack Extension in Fiberglass Reinforced Plastics," T and M Report, University of Illinois, vol. 275, 1965.